Transportation Research Part B 45 (2011) 507–533

Contents lists available at ScienceDirect

Transportation Research Part B

journal homepage: www.elsevier.com/locate/trb

Stochastic cell transmission model (SCTM): A stochastic dynamic traffic model for traffic state surveillance and assignment

A. Sumalee [a,*], R.X. Zhong [a], T.L. Pan [a], W.Y. Szeto [b]

[a] Department of Civil and Structural Engineering, The Hong Kong Polytechnic University, Hong Kong SAR, China
[b] Department of Civil Engineering, The University of Hong Kong, Hong Kong SAR, China

ARTICLE INFO

Article history:
Received 12 June 2009
Received in revised form 22 September 2010
Accepted 24 September 2010

Keywords:
Cell transmission model
discrete time bilinear stochastic system
Dynamic link model
Macroscopic stochastic dynamic traffic model
Traffic flow

ABSTRACT

The paper proposes a first-order macroscopic stochastic dynamic traffic model, namely the stochastic cell transmission model (SCTM), to model traffic flow density on freeway segments with stochastic demand and supply. The SCTM consists of five operational modes corresponding to different congestion levels of the freeway segment. Each mode is formulated as a discrete time bilinear stochastic system. A set of probabilistic conditions is proposed to characterize the probability of occurrence of each mode. The overall effect of the five modes is estimated by the joint traffic density which is derived from the theory of finite mixture distribution. The SCTM captures not only the mean and standard deviation (SD) of density of the traffic flow, but also the propagation of SD over time and space. The SCTM is tested with a hypothetical freeway corridor simulation and an empirical study. The simulation results are compared against the means and SDs of traffic densities obtained from the Monte Carlo Simulation (MCS) of the modified cell transmission model (MCTM). An approximately two-miles freeway segment of Interstate 210 West (I-210W) in Los Ageles, Southern California, is chosen for the empirical study. Traffic data is obtained from the Performance Measurement System (PeMS). The stochastic parameters of the SCTM are calibrated against the flow–density empirical data of I-210W. Both the SCTM and the MCS of the MCTM are tested. A discussion of the computational efficiency and the accuracy issues of the two methods is provided based on the empirical results. Both the numerical simulation results and the empirical results confirm that the SCTM is capable of accurately estimating the means and SDs of the freeway densities as compared to the MCS.

1. Motivation and introduction

Dynamic traffic flow models are one of the key components of dynamic traffic assignment (DTA) as well as real-time traffic control and management. To model the complex freeway traffic, many efforts have been made to establish and validate both microscopic (*e.g.* car-following) and macroscopic (*e.g.* hydrodynamics-based) models. However, many of these models are too computationally demanding for online estimation of traffic states for a large-scale road network. A comparative study of the four macroscopic link models that are widely used in DTA is given by Nie and Zhang (2005). It is found in the paper that these macroscopic link models would produce the same traffic assignment result unless there is a shockwave.

* Corresponding author. Tel.: +852 3400 3963; fax: +852 2334 6389.
E-mail addresses: ceasumal@polyu.edu.hk (A. Sumalee), cezhong@gmail.com (R.X. Zhong), glorious9009@gmail.com (T.L. Pan), ceszeto@hku.hk (W.Y. Szeto).

0191-2615/$ - see front matter © 2010 Elsevier Ltd. All rights reserved.
doi:10.1016/j.trb.2010.09.006

Among the macroscopic traffic flow models, Lighthill–Whitham–Richards (LWR) model would be the most popular and most-cited one. In terms of fluid dynamics, the traffic dynamics of a freeway segment modeled by the LWR model is governed by the following two equations.

$$\frac{\partial \rho(x,t)}{\partial t} + \frac{\partial f(x,t)}{\partial x} = v_+(x,t) - v_-(x,t), \qquad f(x,t) = F(\rho(x,t)), \tag{1}$$

where x, t represents position (measured in the direction of traffic flow) and time, respectively. $\rho(x, t)$ and $f(x, t)$ denote the traffic density and the traffic flow (as functions of location x and time t), respectively. $v_{\pm}(x, t)$ are the source terms which may be due to ramp flows with the plus sign denotes on-ramps and the minus sign denotes off-ramps (Schönhof and Helbing, 2007). The first equation of (1) is the principle of conservation of vehicles, which is followed from fluid mechanics. The second equation of (1) is a flow–density relationship which is also known as the "fundamental diagram". There are several ways to introduce stochastic elements to the LWR modeling framework, e.g.

1. stochastic initial and boundary conditions,
2. stochastic source terms, and
3. stochastic speed–density relationship or fundamental diagram.

Some dynamic traffic flow models (*e.g.* the cell transmission model (CTM) proposed by Daganzo (1994, 1995), the Modified Cell Transmission Model (MCTM) proposed by Muñoz et al. (2003), and the Enhanced Lagged CTM proposed by Szeto (2008)), which discretize the LWR model (or its simplified version) in both time and space, were shown to be computationally efficient and easy to analyze yet capture many important traffic phenomena, such as queue build-up and dissipation, and backward propagation of congestion waves. In general, the original LWR model and other first-order macroscopic traffic flow models derived from it, *e.g.* CTM, have a common assumption of a steady-state speed–density relationship which does not allow fluctuations around the equilibrium (nominal) fundamental flow–density diagram, or these models adopt a number of deterministic parameters (*e.g.* free-flow speed, jam density, capacity, etc.).

However, research and empirical studies on the fundamental flow–density diagram have revealed that the fundamental flow–density diagram admits large variations (see Fig. 1) due to the congestion, driving behavior, etc. (*e.g.* Kim and Zhang, 2008; Wang et al., 2009; Li et al., 2009 and the references therein). Microscopic and macroscopic modeling approaches have been proposed to model and interpret this phenomenon. In the microscopic approach, this phenomenon has been interpreted as the effects of anticipation, strong correlations in the vehicle motion on different lanes, delay in the driving adaptation or safe time-gap variations (*e.g.* Ngoduy, in press and the references therein). In the macroscopic approach, the phenomenon has been modeled as a diffusion coefficient to reproduce significant elements of the synchronized traffic flow, the interactions between several vehicle classes (*e.g.* trucks and cars), randomness in driving behavior, and adverse weather conditions, etc. (Chen et al., 2001; Ngoduy, in press). As mentioned by Geistefeldt and Brilon (2009), the stochastic features of freeway capacity can be revealed by analyzing the transition of traffic flow from free flow to congested conditions, which is referred to as a traffic breakdown. A traffic breakdown indicates that the traffic demand has exceeded the capacity, the variability of these breakdown volumes indicates the randomness of freeway capacity. Therefore, "stochastic" traffic flow models, *e.g.* (Boel and Mihaylova, 2006; Kim and Zhang, 2008; Li et al., 2009), were developed to capture random traffic states of freeways. This can be considered as attempts to introduce the stochasticity into the speed–density relationship (or fundamental diagram) which corresponds to the third component of the stochastic LWR modeling discussed earlier.

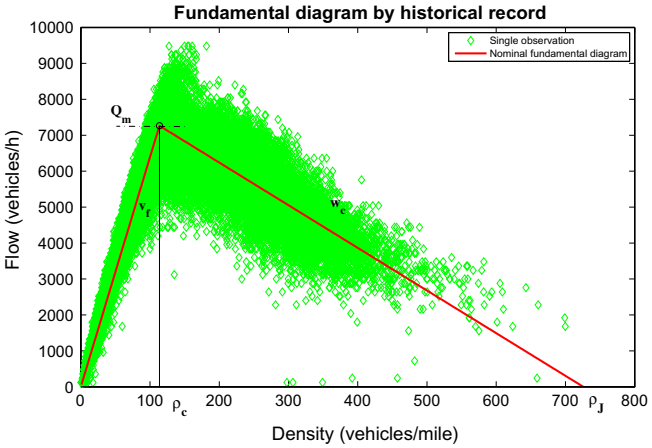

Fig. 1. A fundamental flow–density diagram of traffic flow.

In fact, the other kind of uncertainty is travel demand variability, which is always regarded as recurrent uncertainty or disturbance in traffic flow dynamics. Corresponding to the LWR model, the demand uncertainty would represent the stochastic boundary conditions and source terms (this corresponds to the first and second components of the stochastic LWR modeling discussed earlier). By allowing the stochastic demand input, the dynamic link model can better capture the possible future uncertainty of the travel demand which can enhance the application of the model with short and medium term operation/planning. Therefore, this paper aims to extend the CTM to estimate the stochastic freeway traffic states under stochastic fundamental flow–density diagrams as well as the stochastic travel demand, wherein the deterministic LWR and its extensions fail.

The CTM proposed by Daganzo (1994, 1995) defines piecewise affine sending and receiving functions of traffic flow to describe interactions between adjacent freeway cells as well as shockwaves. For the purposes of developing surveillance, assignment and control strategies on freeways, it is also important to explicitly model the randomness of the traffic state evolution (*e.g.* Peeta and Zhou, 2006 and Friesz et al., 2008 and the references therein). This randomness can be reflected in the model via some stochastic process of the parameters governing the sending and receiving functions (Boel and Mihaylova, 2006). To extend the CTM to deal with the stochastic elements, the simplest approach is to apply the Monte Carlo Simulation method to the CTM. Based on the switching-mode model (SMM) (*i.e.* a simplified version of MCTM distinguishing between the free-flow mode and the congestion mode) and a sequential Monte Carlo algorithm (*i.e.* the so-called mixture Kalman filtering), Sun et al. (2003) proposed a freeway traffic estimator. As a drawback of the Monte Carlo Simulation (MCS), the model may suffer from high computational cost.

A stochastic compositional model for freeway traffic flows was proposed by Boel and Mihaylova (2006). This model extends the CTM by defining sending and receiving functions as random variables, and specifying the dynamics of the average speed in each cell. In this model, the traffic states are divided into two extreme cases: very light traffic conditions and extremely congested conditions where the sending functions are assumed to follow Binomial and Gaussian distributions respectively. However, the intermediate cases between very light traffic and very dense traffic are not well defined. Based on the above dynamic traffic model, a particle filtering (PF) framework was proposed to estimate both traffic density and speed (Mihaylova et al., 2007). The implemented PF performs well with a small number of particles (which can be regarded as samples in the MCS) in the case of the light traffic condition. However, obtaining a good estimation in the case of the dense traffic condition can be computational expensive. It is also difficult to characterize in general the PF accuracy and complexity because they highly depend on the road structure and the traffic conditions (Mihaylova et al., 2007).

In this paper, we develop a stochastic cell transmission model (SCTM) to describe the macroscopic dynamics of the traffic flow under demand and supply uncertainties. The SCTM extends the CTM by defining the parameters governing the sending and receiving functions explicitly as random variables. The stochascities of the sending and receiving functions are governed by the random parameters of the piecewise flow–density diagram, *i.e.* free-flow speed, jam-density, and backward wave speed. In addition, the SCTM also allows the inflow demand to be stochastic. The stochastic elements in our framework are described by some wide-sense stationary, second-order processes consisting of uncorrelated random vectors with known mean and variance. These elements can vary with time depending on the availability of on-line measurements and the locations of the cells.

The proposed model avoids the non-linearities in the original CTM by using the SMM[1] with five possible traffic modes (or states) previously proposed by Muñoz et al. (2003) and Sun et al. (2003). The SMM is a simplified version of the MCTM and will be described in detail later. Each of the traffic modes (or states) of the SCTM is then redefined as a discrete time stochastic bilinear system (*e.g.* Mohler, 1973 and Tuan, 1985). Since the SCTM operates under a stochastic environment, all five modes are possible at each time step. This will cause a problem of the curses of dimensionality, *i.e.* the dimension of the problem increases exponentially with respect to time, if we track all the modes at each time step. To this end, a set of probabilistic conditions is defined for approximating the joint traffic density following the theory of finite mixture distribution to avoid the curses of dimensionality.

Freeway traffic data is often available in the form of occupancy and volume measurements collected from loop detectors embedded in the pavement. In conjunction with effective vehicle length data, these measurements can be converted into macroscopic quantities such as traffic density and speed. Loop detector data sets are often incomplete, or contain bad samples. However, for the purpose of dynamic traffic assignment (DTA) and ramp metering control strategies, such as ALINEA (*e.g.* Gomes and Horowitz, 2006), accurate traffic OD information and density information are required in order to effectively direct traffic and regulate on-ramp inflows to the freeway. It is thus essential to reconstruct the missing traffic measurement data. The SCTM provides us a tool to reconstruct the traffic data which is adaptive to changing stochastic external conditions (supply and demand uncertainties) such as: weather and lighting conditions, percentage of trucks, variable speed limits applied, and variation of travel demand. Numerical and empirical tests involve comparing the means and standard deviations (SDs) of the dynamic traffic densities as approximated by the SCTM and the Monte Carlo Simulation with the density-based equivalent of CTM. In addition, a numerical test is also conducted to illustrate the feature of the proposed model in capturing the propagation of the uncertainty through space and time. All the tests give satisfactory results which prove that the SCTM is computationally efficient and is suitable for real-time traffic monitoring and control applications.

[1] A simpler version of the SMM was first proposed by Zhang et al. (1996) from a traffic control context. In that paper, the traffic flow were modeled by different modes without specifying the various types of waves systematically.

The outline of the paper is as follows: Section 2 gives a brief review on the MCTM and the SMM. The SCTM is formulated in Section 3. Numerical tests of the SCTM are conducted in Section 4. The empirical study is provided in Section 5. Lastly, conclusions and future research issues are highlighted in Section 6.

2. The MCTM and the SMM

The modified cell transmission model (MCTM) was developed by Muñoz et al. (2003). This model uses cell densities instead of cell occupancies which permits the CTM to adopt non-uniform cell lengths and leads to greater flexibility in partitioning freeways. In the MCTM, the density of cell i evolves according to the conservation of vehicles:

$$\rho_i(k+1) = \rho_i(k) + \frac{T_s}{l_i}\left(q_{i,in}(k) - q_{i,out}(k)\right), \tag{2}$$

where $\rho_i(k)$ is the vehicle density of cell i at time index k, $q_{i,in}(k)$ and $q_{i,out}(k)$ are the total flows (in vehicles per unit time) entering and leaving cell i during the time interval $[k\,T_s, (k+1)T_s)$ respectively, T_s is the sampling duration, and l_i is the length of cell i. The model parameters, including the free-flow speed v_f, the backward congestion wave speed w_c, the maximum allowable flow Q_M, the jam density ρ_J, and the critical density ρ_c, are depicted in the trapezoidal fundamental diagram of Fig. 2. These parameters can vary from cell to cell over time.

Following Daganzo (1994, 1995), $q_i(k)$ is determined by taking the minimum of two quantities:

$$q_{i,in}(k) = \min(S_{i-1}(k), R_i(k)), \tag{3}$$

where $S_{i-1}(k) = \min(v_{f,i-1}(k)\rho_{i-1}(k), Q_{M,i-1}(k))$ is the maximum flow supplied by cell $i-1$ under the free-flow condition, over the interval $[k, k+1)$, and $R_i(k) = \min(Q_{M,i}(k), w_{c,i}(k)(\rho_{J,i}(k) - \rho_i(k)))$, is the maximum flow received by cell i under the congested condition over the same time interval. (2) and (3) are the density-based equivalents of those described in Daganzo (1994).

Although the MCTM is much simpler than many other higher order hydrodynamics-based partial differential models, the nonlinear nature of the flow–density relationship due to (3) still makes the MCTM difficult to be analyzed and used as a basis for the design of traffic controllers (Muñoz et al., 2003; Gomes et al., 2008). To avoid the nonlinearity, the switching-mode model (SMM) was proposed by Muñoz et al. (2003). The SMM is a hybrid system (or switched linear system) that switches among different sets of linear difference equations (representing different traffic states of the freeway), depending on the mainline boundary data and the congestion status of the cells in a freeway segment. The SMM formulation avoids the nonlinearity of the CTM at the cost of using the same triangular flow–density relationship for all the cells along the whole freeway segment, and introducing the switching condition based on the following atmost-one-wavefront assumption:

Assumption 2.1. (Muñoz et al., 2003) There is at most one wavefront in the freeway segment.

Based on the above assumption, five modes are defined in the state space representation (see Fig. 3):

1. "Free flow-Free flow (FF)" (Fig. 3a).
2. "Congestion – Congestion (CC)" (Fig. 3b).
3. "Congestion – Free flow (CF)" (Fig. 3c).
4. "Free flow-Congestion 1 (FC1)" (Fig. 3d).
5. "Free flow – Congestion 2 (FC2)" (Fig. 3e).

A wavefront is assumed to be located at the boundary between the two cells at time k. Among these five modes, the FF and CC modes are steady-state modes while the others are transient modes. The two modes of "Free flow – Congestion" are determined by the relative magnitudes of the supplied flow of the last uncongested cell upstream of the wave front and the receiving flow of the first congested cell downstream of the wave front. If the former is smaller, the SMM is in the FC1 mode,

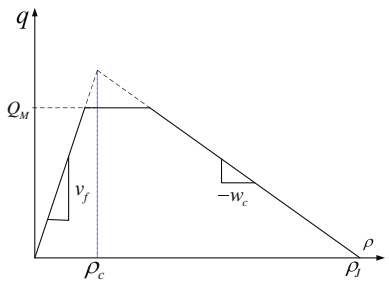

Fig. 2. A trapezoidal fundamental diagram for the modified cell transmission model.

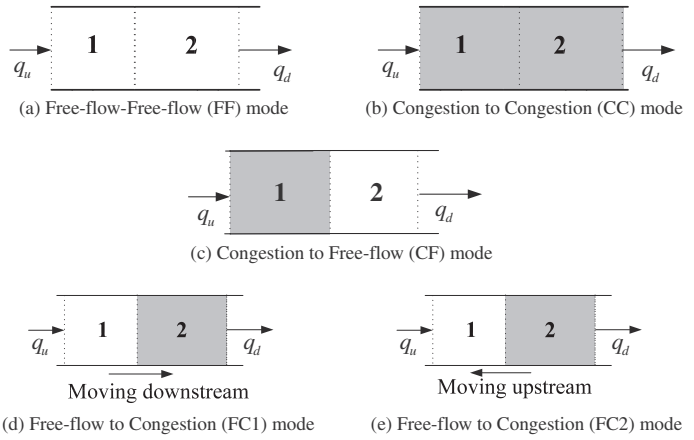

Fig. 3. Five traffic operational modes for a freeway segment with two cells.

otherwise it is in the FC2 mode. In the SMM, the mode of the model is determined following a set of traffic density based switching criteria in which only one mode is activated at each time step.

3. The stochastic cell transmission model

3.1. The overall framework of the SCTM

As previously described, in Muñoz et al. (2003), Sun et al. (2003), the MCTM has been piecewise-linearized to obtain the SMM with five operational modes for a freeway segment based on Assumption 2.1. From the traffic control context, the linear structure of the SMM lends the advantage of simplifying control analysis, control design, and data-estimation design methods. From the traffic flow simulation context, Assumption 2.1 simplifies the traffic state of the freeway segment which increases the computational efficiency. To utilize the SMM, we need to ensure that the traffic dynamics of a freeway segment can be accurately described by the five modes. However, Assumption 2.1 cannot be fulfilled for general freeway segments except some special cases. A simple way to fulfill the assumption is to divide a freeway corridor into several short segments wherein each of these segments is modeled by one subsystem consisting of two cells. The traffic state of each subsystem then can be covered by the five modes (i.e. the atmost one-wavefront assumption is satisfied under the deterministic environment). In this paper, we extend the CTM to simulate the traffic dynamics of a freeway corridor with stochastic demand and supply by this interconnected subsystems approach as depicted in Fig. 4. To begin with, we explain the dynamics within one SCTM subsystem.

A freeway segment with one on-ramp and one off-ramp[2] is modeled as one SCTM subsystem, whose block diagram is depicted in Fig. 4a. We follow the concept of operational modes utilized in the SMM. However, due to the stochastic supply and demand, the wavefront is uncertain, which implies that within one subsystem all the five modes are possible (hence five probabilistic events) but with different probabilities of occurrence. We denote these probabilities as: $P_{FF}(k)$, $P_{CC}(k)$, $P_{CF}(k)$, $P_{FC1}(k)$, and $P_{FC2}(k)$, where $P_s(k)$ is the probability of mode $s \in \{FF, CC, CF, FC1, FC2\}$ to occur at time index k. To this end, we update the dynamics of the SCTM as depicted in Fig. 5, where the overall effect of the five modes is defined as the joint (or "actual") traffic density. The probabilities of occurrence in conjunction with the density vectors of the five modes are used to define the probability density function (PDF) of the joint traffic density vector $\bar{\rho}(k)$, which is approximated by a finite mixture approximation of the probability density functions of the five modes. Its mean $E(\bar{\rho}(k)|\theta(k))$ and covariance matrix $Var(\bar{\rho}(k)|\theta(k))$ can be obtained by the theory of finite mixture distribution which will be explained in Section 3.3, where $\theta(k) = \{\theta_s(k)\}$, $\theta_s(k) = (\rho_s(k), P_s(k))$, and $\rho_s(k)$ denotes the vector of cell densities of mode s.

To sum up, the SCTM subsystem accepts the random inflows (uncertain demand) as well as random parameters of the fundamental flow–density diagram (uncertain supply functions) with known means and variances of the freeway segment as exogenous inputs, and then calculates the means and variances of the joint traffic densities, outflow of the freeway segment, and probabilities of its operational modes as shown in Fig. 4. We emphasize here that:

- First, the current framework does not rely on Assumption 2.1. This assumption is only used to define the operational modes for one SCTM subsystem following the SMM. A freeway corridor as depicted in Fig. 4 can have several uncertain wavefronts.

[2] In this paper, we do not consider the dynamics of the on-/off-ramps, i.e. we do not consider the merge and diverge operations. The on-/off-ramp flows considered here are the measured on-/off-ramp flows.

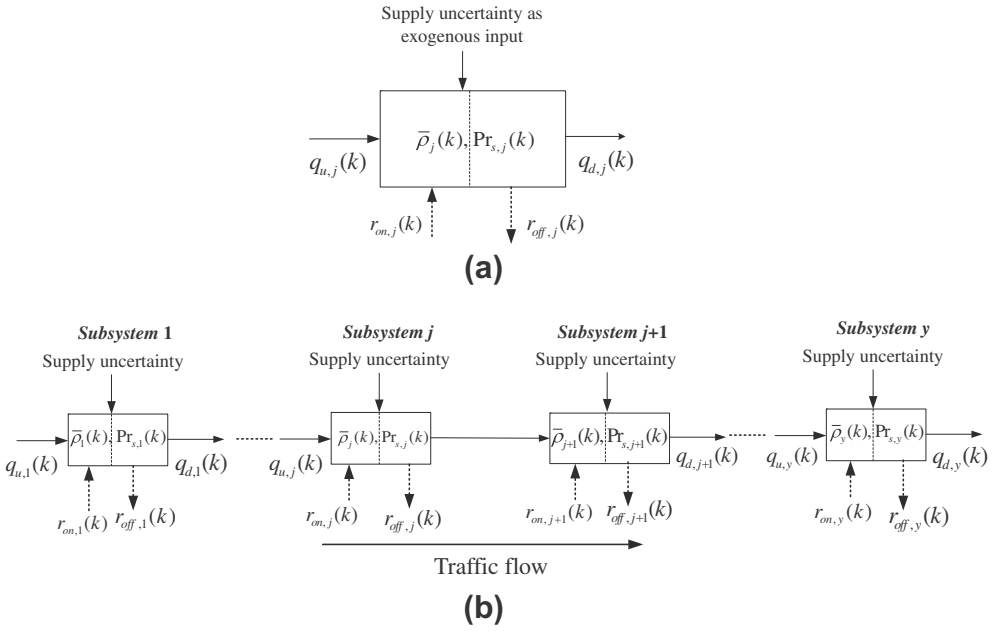

Fig. 4. An interconnected SCTM approach to model a freeway corridor: (a) a short segment as one SCTM subsystem, segment variables, and segment inputs; (b) a freeway corridor as interconnected SCTM subsystems.

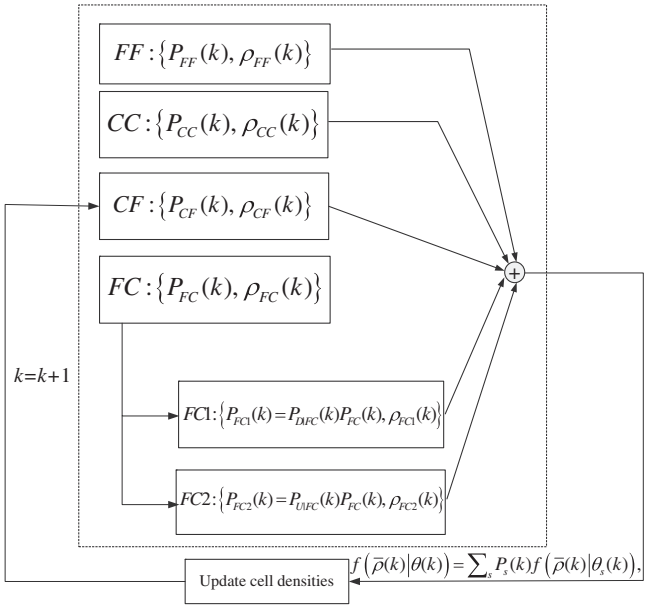

Fig. 5. The dynamics of the stochastic cell transmission model.

- Second, the uncertain wavefront concept is converted into several probabilistic operational modes in the current framework. The uncertain wavefront is described by the probabilities of occurrence of these operational modes.

As we model a freeway corridor by cascading several SCTM subsystems and each SCTM subsystem admits several exogenous inputs, we need to define a number of boundary variables to simulate the stretch SCTM system for a freeway corridor: (a) flow at the stretch origin $q_{u,1}$, (b) flow at the stretch destination $q_{d,y}$, (c) measured on-ramp flows $r_{on,j}$ (if any), and measured off-ramp flows $r_{off,j}$ (if any), (d) the uncertain supply functions of each cells. Similar idea has been adopted in Wang et al. (2007). Inside the stretch SCTM system, each of these subsystems accepts the outflow from the upstream segment as inflow.

With respect to the above framework, five key issues are needed to be addressed. The fist issue is to define the demand and supply uncertainties. The second issue is to define the probabilities of occurrence of the five operational modes and to approximate the PDF of the joint traffic density vector by a finite mixture distribution of the PDFs of the five operational modes. The third issue is to model the dynamics of the five operational modes. The means and auto-correlations of the dynamics of the five operational modes are needed to be evaluated. Finally, we need to define the flow propagation between two adjacent SCTM subsystems and the implementation of the SCTM for traffic state estimation.

3.2. Formulation of demand and supply uncertainties

From the analysis in the previous subsection, to evaluate the stochastic traffic dynamics, we need to define the probabilities and the traffic flow dynamics for the five modes. To begin with, let's first specify the demand and supply uncertainties considered in this paper. Consider a freeway segment consisting of 2 cells and one on-ramp and one off-ramp as depicted in Fig. 4a. We denote the traffic state at time index $k \geqslant 0$ as the traffic density $\rho(k) = (\rho_1(k), \rho_2(k))^T$, and $u(k) = (q_u(k), r_{on}(k), r_{off}(k), q_d(k))^T$ is comprised of system inflow and outflow at time index k. $r_{on}(k)$ and $r_{off}(k)$ are the measured on-ramp and off-ramp flows at time index k, respectively. $q_u(k)$ and $q_d(k)$ are respectively the (measured) upstream and downstream boundary flows at time index k, and $\rho_u(k)$, and $\rho_d(k)$ are densities defined correspondingly. To save notations, the notations for the five parameters in Fig. 2 are also used for representing the corresponding five vectors in the SCTM when there is no ambiguity. To be more specific, $v_f = (v_{f,1}, v_{f,2})^T$ is the vector of free-flow speeds, $\rho_c = (\rho_{c,1}, \rho_{c,2})^T$ is the vector of critical densities, $w_c = (w_{c,1}, w_{c,2})^T$ is the vector of backward congestion wave speeds, $\rho_J = (\rho_{J,1}, \rho_{J,2})^T$ is the vector of jam densities, and $Q_M = (Q_{M,1}, Q_{M,2})^T$ is the vector of maximum flow rates. According to the triangular fundamental diagram of a given cell, only three among the five system parameters are independent variables. We denote an independent set of the system parameters in a compact form as $\Gamma = col(v_f, w_c, Q_M)$. In the real world, the system parameter vector Γ admits uncertainties. We assume that the system parameter vector is perturbed by certain noise sequence as follows:

$$\Gamma(k) = \Gamma_0 + \xi^{\Gamma}(k), \tag{4}$$

where $\Gamma(k)$ is the system parameter vector for time k, Γ_0 is the nominal value of the system parameters, and $\xi^{\Gamma}(k)$ is the noise vector for system parameters at time index k. Note that $\{\xi^{\Gamma}(k)\}_{k\in N}$ is a second-order wide-sense stationary (WSS) process[3] to be specified later. Also, we assume the travel demand to be a random vector in the form

$$u_d(k) = u_0(k) + \xi_u(k), \tag{5}$$

where $u_d(k) = (q_u(k), r_b(k))^T$, $u_0(k)$ is the nominal calibrated travel demand vector for time index k, and $\xi_u(k)$ is the demand noise at time index k. $\{\xi_u(k)\}_{k\in N}$ is a second-order WSS process to be specified later. Without loss of generality, all the noise sequences and initial conditions are assumed to follow Gaussian (white-noise) processes.

For the demand side, we assume the noise sequence $\{\xi_u(k)\}_{k\in N}$ in the control input to be a zero-mean Gaussian random process:

$$E(\xi_u(k)) = 0, E\left(\xi_u(k)\xi_u^T(t)\right) = \begin{cases} \Omega_u, & \text{if } k = t; \\ 0, & \text{otherwise}, \end{cases} \tag{6}$$

where k and t are time indices. Similarly, for the supply side we assume that the noise $\xi^{\Gamma}(k)$ and the initial state $\rho(0)$ of the system satisfy the following conditions:

1. The noise $\xi^{\Gamma}(k)$ can be described by a zero-mean Gaussian random process. For any $k \geqslant 0$ and $t \geqslant 0$, the following equations are satisfied:

$$E(\xi^{\Gamma}(k)) = 0, E\left(\xi^{\Gamma}(k)\left(\xi^{\Gamma}(t)\right)^T\right) = \begin{cases} \Omega_{\Gamma}, & \text{if } k = t; \\ 0, & \text{otherwise}. \end{cases} \tag{7}$$

We also assume that, the components of the vector $\xi^{\Gamma}(k)$ are mutually independent for any $k \geqslant 0$, or the matrix Ω_{Γ} is a diagonal semi-positive definite matrix.
2. The components of the initial traffic density vector $\rho(0)$ are mutually independent and normally distributed.
3. $\rho(0)$ and $\xi^{\Gamma}(k)$ are uncorrelated to each other for any $k \in N$.

Remark 3.1. As mentioned before, only three among the five system parameters are independent. For illustration purposes, consider cell i with a triangular flow–density relationship and let $(v_{f,i}, w_{c,i}, Q_{M,i})$ be the independent set of the parameters for cell i. $\rho_{c,i}$ and $\rho_{J,i}$ can then be determined by $v_{f,i}$, $w_{c,i}$, and $Q_{M,i}$. Let $x_i = (v_{f,i}, w_{c,i}, Q_{M,i})^T$, then $\rho_{c,i} = g(x_i) = \frac{Q_{M,i}}{v_{f,i}}$. Applying Taylor expansion to $g(x_i)$ at x_0 yields

$$\rho_{c,i} = g(x_i) = g(x_0) + (x_i - x_0)^T \nabla g(x_0) + \frac{1}{2}(x_i - x_0)^T H(x_0)(x_i - x_0) + \cdots,$$

[3] A random process $x(k)$ is said to be wide-sense stationary (WSS) if $E(x(k)) = c$ and $E(x(l)x^T(k)) = \Omega_x(k - l) = \Omega_x(\tau)$, where c is a constant vector and $\Omega_x(\cdot)$ is the correlation matrix of the process, and $\tau = k - l$ is the time lag.

where $\nabla g(x_0)$ is the gradient of g at x_0 and $H(x_0)$ is the corresponding Hessian matrix. Take

$$g(x_i) \approx g(x_0) + (x_i - x_0)^T \nabla g(x_0) + \frac{1}{2}(x_i - x_0)^T H(x_0)(x_i - x_0). \tag{8}$$

Since x_i is a vector with its components mutually independent and its mean and variance are given in the above assumptions, we can approximate the mean of $\rho_{c,i}$ by taking expectation on both sides of (8), and the variance can be obtained respectively. Notice that if the first-order approximation is used in (8), $\rho_{c,i}$ is normally distributed when we assume that x_i is governed by a normal distribution. Similarly, we can approximate the mean and variance for $\rho_{J,i} = \frac{Q_{M,i}}{w_{c,i}} + \frac{Q_{M,i}}{v_{f,i}}$.

In what follows, we denote the vector of system parameters as $\Phi(k) = col(v_f(k), w_c(k), Q_M(k), \rho_c(k), \rho_J(k))$.

3.3. Dynamic process of the SCTM and probabilistic conditions

As mentioned, we need to specify the probabilities of the five modes at each time step to evaluate the stochastic traffic flow. The probabilities of the two steady-state modes, i.e. FF, and CC modes, to occur can be determined as follows: FF mode:

$$P_{FF}(k) \triangleq \Pr\Big(\rho_u(k-1) < \rho_{c,1}(k-1) \cap \rho_d(k-1) < \rho_{c,2}(k-1)\Big), \text{and} \tag{9}$$

CC mode:

$$P_{CC}(k) \triangleq \Pr\Big(\rho_u(k-1) \geqslant \rho_{c,1}(k-1) \cap \rho_d(k-1) \geqslant \rho_{c,2}(k-1)\Big). \tag{10}$$

As mentioned before, the shockwave exists only in the three transient modes, i.e. CF, FC1, and FC2 modes. We define the following probability to capture the probability of the CF mode to occur as:

$$P_{CF}(k) \triangleq \Pr\Big(\rho_u(k-1) \geqslant \rho_{c,1}(k-1) \cap \rho_d(k-1) < \rho_{c,2}(k-1)\Big). \tag{11}$$

Let $P_{FC}(k)$ be the probability of the FC mode occurring at time k. Then,

$$P_{FC}(k) \triangleq 1 - (P_{FF}(k) + P_{CC}(k) + P_{CF}(k)), \tag{12}$$

with the wavefront moving downstream (event D) as

$$P_{D|FC}(k) \triangleq \Pr\Big(v_{f,1}(k-1)\bar{\rho}_1(k-1) \leqslant w_2(k-1)\Big(\rho_{J,2}(k-1) - \bar{\rho}_2(k-1)\Big)\Big),$$

and the probability of the wavefront moving upstream (event U) is $P_{U|FC}(k) = 1 - P_{D|FC}(k)$, Then the probabilities of the FC1 and FC2 modes to occur at time step k are:

- FC1 mode:

$$P_{FC1}(k) \triangleq P_{D|FC}(k) P_{FC}(k), \tag{13}$$

- FC2 mode:

$$P_{FC2}(k) \triangleq P_{U|FC}(k) P_{FC}(k). \tag{14}$$

With the above definitions of probabilities of occurrence of the five operational modes, we need to address the problem that how to estimate (or approximate) the overall effect of the five possible operational modes (or the joint traffic density) given their PDFs. In this paper, we provide a finite mixture distribution approach to solve the above question, i.e. the overall effect of the five possible operational modes is estimated (or approximated) by a finite sum of known PDFs. The probability density function (PDF) of the joint traffic density $f(\bar{\rho}(k)|\theta(k))$ can be approximated by the following finite mixture distribution (Frühwirth-Schnatter, 2006):

$$f(\bar{\rho}(k)|\theta(k)) = \sum_s P_s(k) f(\bar{\rho}(k)|\theta_s(k)), \tag{15}$$

where f is the PDF of the joint traffic density $\bar{\rho}(k)$, the parameter set is defined as $\sum_s P_s(k) = 1,\ \{\theta(k)\} = \{\theta_s(k)\},\ \theta_s(k) = (P_s(k),\ \rho_s(k)),\ \rho_s(k)$ denotes the vector of cell densities of mode s at time k, and $P_s(k)$ is defined by (9)–(14) with $s = \{FF, CC, CF, FC1, FC2\}$.

Under the mixture model (15), the expectation $E(\bar{\rho}(k)|\theta(k))$ is obviously given by

$$E(\bar{\rho}(k)|\theta(k)) = \sum_s P_s(k) E(\bar{\rho}(k)|\theta_s(k)) = \sum_s P_s(k) E(\rho_s(k)). \tag{16}$$

Let $\mu_s(k) = E(\rho_s(k))$ and $\mu(k) = E(\bar{\rho}(k)|\theta(k))$. Then we have $\mu(k) = \sum_s P_s(k)\mu_s(k)$. To evaluate the covariance matrix $Var(\bar{\rho}(k)|\theta(k))$, we define the covariance matrix of $\rho_s(k)$ as

$$\psi_s(k) = E\Big((\rho_s(k) - \mu_s(k))(\rho_s(k) - \mu_s(k))^T\Big).$$

Then the covariance matrix $Var(\bar{\rho}(k)|\theta(k))$ can be evaluated as:

$$Var(\bar{\rho}(k)|\theta(k)) = \sum_s P_s(k)\left(\psi_s(k) + \mu_s(k)\mu_s^T(k)\right) - \mu(k)\mu^T(k). \tag{17}$$

If the mean and covariance matrix are defined, the "joint traffic density" is well defined for a second-order random process. As the probabilities of the five modes are already defined, we need to obtain the mean of the cell traffic density vector $\mu_s(k)$ and the covariance matrix $\psi_s(k)$ for each mode s at each time step k.

3.4. The SCTM as a class of stochastic bilinear system

To allow the analysis to be more systematic and compact, we define the density update equations of each mode in the form of a dynamic system. Due to the multiplicative effect of the system parameters in the SCTM, such as v_f, w_c, and ρ_J, our system is no longer a linear system. Nevertheless, the SCTM can be reformulated as a class of discrete time stochastic bilinear system in the form of (18) below. However, instead of specifying the system parameter vector $\Phi(k)$ of the freeway segment as internal dynamics (or system matrices) as what has been done in Muñoz et al. (2003), we take the system parameter vector as an exogenous input to the system together with the inflow vector $u(k)$.

$$\rho(k+1) = \left(A_0 + \sum_{i=1}^{p} A_i\omega_i(k)\right)\rho(k) + \left(B_0 + \sum_{i=1}^{p} B_i\omega_i(k)\right)\lambda(k) + Bu(k),\ \ k \in N, \tag{18}$$

where B, A_i, B_i, $i = 0,1,\ldots,p$ are constant matrices to be defined later, $\omega_i(k)$, $\forall k \in N$ are second-order processes consisting of mutually uncorrelated real-valued random variables. The sequence of random vectors $\lambda(k)$, $\forall k \in N$ in (18) is viewed as a disturbance signal. The disturbance of the system equations in (18) consists of two parts, $B_0\lambda(k)$ and $\sum_{i=1}^{p} B_i\omega_i(k)\lambda(k)$. We call the first term the drift component and the second the diffusion component of the disturbance. The presence of both types of multiplicative disturbances in (18) (*i.e.,* the drift and the diffusion terms) is an essential feature of our SCTM. As to be shown later, it allows for parameter excitations in both the state and the disturbance input matrices. As we consider one SCTM subsystem consisting of two cells only, which implies $p = 2$. We specify the actual formulation of (18) under each mode of the SCTM as:

In the FF mode, we set $\omega_i(k)$ to be the free-flow speed $v_{f,i}(k)$ in (18), and the state equation can be represented as:

$$\rho(k+1) = \left(I + \sum_{i=1}^{2} A_i v_{f,i}(k)\right)\rho(k) + Bu(k), \tag{19}$$

where

$$A_1 = \begin{bmatrix} -\frac{T_s}{l_1} & 0 \\ \frac{T_s}{l_2} & 0 \end{bmatrix},\quad A_2 = \begin{bmatrix} 0 & 0 \\ 0 & -\frac{T_s}{l_2} \end{bmatrix},\quad B = \begin{bmatrix} \frac{T_s}{l_1} & \frac{T_s}{l_1} & 0 & 0 \\ 0 & 0 & 0 & 0 \end{bmatrix}.$$

Eq. (19) is a special case of (18) with B_i, $i = 1, 2$ be null matrices and $\lambda(k)$ be a null vector. Note that in (19), the free-flow speed $v_{f,i}(k)$ is no longer the internal dynamics but the exogenous noise sequence. Similarly, we can define the other four modes.

In the CC mode, we define $\omega_i(k) = w_{c,i}(k)$ and the vector $\lambda(k) = (\rho_{J,1}(k),\ \rho_{J,2}(k))^T$. The state equation is then

$$\rho(k+1) = \left(I + \sum_{i=1}^{2} A_i w_{c,i}(k)\right)\rho(k) + \sum_{i=1}^{2} B_i w_{c,i}(k)\lambda(k) + Bu(k), \tag{20}$$

where

$$A_1 = \begin{bmatrix} -\frac{T_s}{l_1} & 0 \\ 0 & 0 \end{bmatrix},\quad A_2 = \begin{bmatrix} 0 & \frac{T_s}{l_1} \\ 0 & -\frac{T_s}{l_2} \end{bmatrix},\quad B = \begin{bmatrix} 0 & 0 & 0 & 0 \\ 0 & 0 & -\frac{T_s}{l_2} & -\frac{T_s}{l_2} \end{bmatrix},\quad B_i = -A_i, i = 1,2.$$

In the CF mode, we can define $\omega_1(k) = w_{c,1}(k)$, $\omega_2(k) = v_{f,2}(k)$, and the vector $\lambda(k) = (\rho_{J,1}(k),\ Q_M(k))^T$. The state equation is then

$$\rho(k+1) = \left(I + \sum_{i=1}^{2} A_i\omega_i(k)\right)\rho(k) + \left(B_0 + \sum_{i=1}^{2} B_i\omega_i(k)\right)\lambda(k) + Bu(k), \tag{21}$$

where

$$A_1 = \begin{bmatrix} -\frac{T_s}{l_1} & 0 \\ 0 & 0 \end{bmatrix},\quad A_2 = \begin{bmatrix} 0 & 0 \\ 0 & -\frac{T_s}{l_2} \end{bmatrix},\quad B_0 = \begin{bmatrix} 0 & -\frac{T_s}{l_1} \\ 0 & \frac{T_s}{l_2} \end{bmatrix},\quad B_1 = -A_1,\ \ B_2 = 0_{2\times 2},\ \ B = 0_{2\times 4}.$$

In the FC1 mode, we define $\omega_1(k) = v_{f,1}(k)$, $\omega_2(k) = 0$, and $\lambda(k)$ as a null vector. The state equation is then

$$\rho(k+1) = (I + A_1\omega_1(k))\rho(k) + Bu(k), \tag{22}$$

where

$$A_1 = \begin{bmatrix} -\frac{T_s}{l_1} & 0 \\ \frac{T_s}{l_2} & 0 \end{bmatrix}, \quad B = \begin{bmatrix} \frac{T_s}{l_1} & \frac{T_s}{l_1} & 0 & 0 \\ 0 & 0 & -\frac{T_s}{l_2} & -\frac{T_s}{l_2} \end{bmatrix}.$$

In the FC2 mode, we define $\omega_1(k) = 0$, $\omega_2(k) = w_{c,2}(k)$, and $\lambda(k) = (0, \rho_{J,2}(k))^T$. The state equation is

$$\rho(k+1) = (I + A_2\omega_2(k))\rho(k) + B_2\omega_2(k)\lambda(k) + Bu(k), \tag{23}$$

where

$$A_1 = 0, \quad A_2 = \begin{bmatrix} 0 & \frac{T_s}{l_1} \\ 0 & -\frac{T_s}{l_2} \end{bmatrix}, \; B_1 = 0, \; B_2 = \begin{bmatrix} 0 & -\frac{T_s}{l_1} \\ 0 & \frac{T_s}{l_2} \end{bmatrix}, \; B = \begin{bmatrix} \frac{T_s}{l_1} & \frac{T_s}{l_1} & 0 & 0 \\ 0 & 0 & -\frac{T_s}{l_2} & -\frac{T_s}{l_2} \end{bmatrix}.$$

Thus far, we have represented all the five modes as discrete time bilinear stochastic systems. Since these systems are influenced by second-order random processes, we need to find the means and variance matrices to characterize the traffic density vectors. Each of these state equation systems is associated with each mode of the SCTM as shown in Fig. 5. In order to obtain an analytical approximation of the mean and variance of the mixture distribution of the traffic density at each time step, it is necessary to investigate the statistical properties of the cell density under each mode which will be discussed next.

3.5. Mean and auto-correlation of stochastic traffic densities

The dynamics of $\rho(k)$ can be represented by a discrete time bilinear stochastic system of the form (18), which can be further simplified into the following Markovian representation (Tuan, 1985):

$$\rho(k+1) = (A_0 + W(k))\rho(k) + D(k)\lambda(k) + Bu(k), \tag{24}$$

where the following notations are adopted:

$$W(k) = \sum_{i=1}^{p} A_i\omega_i(k), \quad D(k) = B_0 + \sum_{i=1}^{p} B_i\omega_i(k),$$

where $p = 2$ represents the number of cells within one SCTM subsystem. Eq. (24) exhibits the Markovian property. Thus we can represent the state vector as:

$$\rho(k) = \Phi_w(k,0)\rho(0) + \sum_{t=0}^{k-1} \Phi_w(k,t+1)(Bu(t) + D(t)\lambda(t)), \tag{25}$$

for every $k \geqslant 1$, with $\Phi_w(k,k) = I$ and $\Phi_w(\tau,t) = [A_0 + W(\tau-1)]\cdots[A_0 + W(t)]$ for $\tau > t$. Consider the state sequence generated by (24), and define the mean and the auto-correlation matrix for each $k \geqslant 0$:

$$\varphi(k) = E\{\rho(k)\}, \quad \Omega(k) = E\{\rho(k)\rho^T(k)\}.$$

The existence of $\varphi(k)$ and $\Omega(k)$ for each $k \geqslant 0$ can then be guaranteed by the independence and second-order assumptions. Therefore, by Eq. (25) we obtain the mean as:

$$\varphi(k) = E(\Phi_w(k,0))\varphi(0) + \sum_{t=0}^{k-1} E(\Phi_w(k,t+1))(BE(u(t)) + E(D(t))E(\lambda(t))), \quad \forall k \geqslant 1, \tag{26}$$

where $E(\Phi_w(k,0)) = [A_0 + \sum_{i=1}^{p} E(\omega_i(0))A_i] \ldots [A_0 + \sum_{i=1}^{p} E(\omega_i(k-1))A_i]$, and the term $E(\Phi_w(k,t+1))$ can be similarly defined. Regarding the mixed terms involving both disturbances and states, for each $k \geqslant 0$, by using the independent assumptions, we have:

$$G_1(k) = E\Big([A_0 + W(k)]\varphi(k)u^T(k)B^T\Big) = \left[A_0\varphi(k)(E(u(k)))^T + \sum_{i=1}^{p} A_i\varphi(k)(E(\omega_i(k)u(k)))^T\right]B^T, \tag{27}$$

$$G_2(k) = E\Big(D(k)\lambda(k)u^T(k)B^T\Big) = \left[B_0 + \sum_{i=1}^{p} E(\omega_i(k))B_i\right](E(\lambda(k)))(E(u(k)))^T B^T, \tag{28}$$

$$G_3(k) = E\Big([A_0 + W(k)]\varphi(k)\lambda^T(k)D^T(k)\Big) = \left[A_0\varphi(k) + \sum_{i=1}^{p} E(\omega_i(k))A_i\varphi(k)\right](E(\lambda(k)))^T \cdot \left[B_0 + \sum_{i=1}^{p} E(\omega_i(k))B_i\right]^T + \sum_{i=1}^{p} \gamma_i A_i\varphi(k)(E(\lambda(k)))^T B_i^T, \tag{29}$$

where $\gamma_i = E(\omega_i(k)\omega_i(k)) - (E(\omega_i(k)))^2$. Furthermore, let $G(k) = G_1(k) + G_2(k) + G_3(k)$, and

$$V(k) = G(k) + G^T(k) + B\big(E\big(u(k)u^T(k)\big)\big)B^T + \left[B_0 + \sum_{i=1}^{p} E(\omega_i(k))B_i\right]\big(E\big(\lambda(k)\lambda^T(k)\big)\big)\left[B_0 + \sum_{i=1}^{p} E(\omega_i(k))B_i\right]^T + \sum_{i=1}^{p} \gamma_i B_i\big(E\big(\lambda(k)\lambda^T(k)\big)\big)B_i^T.$$

It can be verified by the independent argument that

$$\begin{aligned}\Omega(k+1) &= E\Big([A_0 + W(k)]\rho(k)\rho^T(k)[A_0 + W(k)]^T\Big) + V(k)\\ &= \left[A_0 + \sum_{i=1}^{p} E(\omega_i(k))A_i\right]\Omega(k)\left[A_0 + \sum_{i=1}^{p} E(\omega_i(k))A_i\right]^T + \sum_{i=1}^{p} \gamma_i A_i \Omega(k) A_i^T + V(k),\ \forall k \geqslant 0,\end{aligned} \tag{30}$$

If we define $F_0 = \left[A_0 + \sum_{i=1}^{p} E(\omega_i(k))A_i\right]$, and $F_i = \sqrt{\gamma_i}A_i$, then (30) is equivalent to

$$\Omega(k+1) = \sum_{i=0}^{p} F_i \Omega(k) F_i^T + V(k), \quad \forall k \geqslant 0. \tag{31}$$

The solution of (31) can be obtained by induction as:

$$\Omega(k) = L^k[\Omega(0)] + \sum_{t=0}^{k-1} L^{k-t-1}[V(t)], \quad \forall k \geqslant 1, \tag{32}$$

where the operator $L[.]$ is defined as

$$L[X] = \sum_{i=0}^{p} F_i X F_i^T, \text{ and } L^t[X] = \sum_{i_t=0}^{p} \cdots \sum_{i_1=0}^{p} F_{i_t} \cdots F_{i_1} X F_{i_t}^T \cdots F_{i_1}^T. \tag{33}$$

To illustrate the mean and variance update of traffic density by the SCTM, we provide a small analytical numerical example in the Appendix of the paper.

3.6. Flow between two adjacent subsystems

To capture the flow propagation, we need to define the random flow across two neighboring SCTM subsystems. Note that the concept of wavefront in the CTM is converted into probabilities of occurrence of the five operational modes in the SCTM. The calculation of flow between two neighboring SCTM subsystems is similar to the calculation of flow between two adjacent cells without wavefront. As depicted in Fig. 6, let subsystems $j-1$ and j are two neighboring SCTM subsystems with two adjacent cells $i-1$ and i, and $S_{j-1}(k)$ is the sending function of subsystem $j-1$ (which is one of the outputs of the SCTM subsystem). Then $S_{j-1}(k) = mix(v_{f,i-1}(k)\rho_{i-1}(k), Q_{i-1}(k))$, where *mix* denotes the finite mixture distribution. The above mixture distribution means that: if the last cell of subsystem $j-1$, is free flowing at time k, the amount of traffic to be sent out is $v_{f,i-1}(k)\rho_{i-1}(k)$, if the last cell of subsystem $j-1$ is congested, the amount to be sent out is $Q_{i-1}(k)$. The probabilities for these two events are $P_1^S(k) = (P_{FF,j-1}(k) + P_{CF,j-1}(k))$, $P_2^S(k) = (P_{FC,j-1}(k) + P_{CC,j-1}(k))$, respectively. To determine the flow received by the downstream SCTM subsystem, we compare this flow profile with the receiving flow of the downstream SCTM subsystem and define the following four events:

- The first cell of the downstream SCTM subsystem is free flow (FF_i) and the sending function $S_{j-1}(k)$ is less than its capacity. In this case, $S_{j-1}(k)$ will be loaded onto the first cell of subsystem j. The corresponding probability is defined as: $P_1(k) = \Pr(FF_i(k) \cap (S_{j-1}(k) < Q_i(k)))$, where $Q_i(k)$ is the capacity of the first cell of the downstream SCTM subsystem.
- The first cell of the downstream SCTM subsystem is free flow (FF_i) and the sending function $S_{j-1}(k)$ is not less than its capacity. In this case, an amount of vehicles equals to $Q_i(k)$ will be loaded. The probability for this event is defined as: $P_2(k) = \Pr(FF_i(k) \cap (S_{j-1}(k) \geqslant Q_i(k)))$.

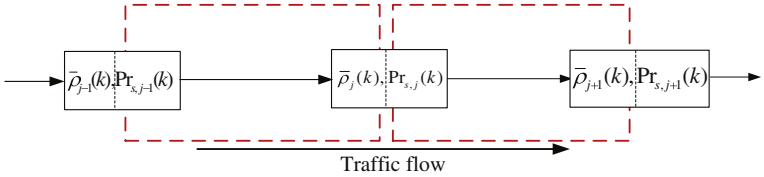

Fig. 6. The interconnected SCTM subsystems approach as paired up two neighboring cells.

- The first cell of the downstream SCTM subsystem is congested (CC_i) and the sending function $S_{j-1}(k)$ is less than its available space $w_i(k)(\rho_{J,i}(k) - \rho_i(k))$. Then, $S_{j-1}(k)$ will be loaded onto the first cell of subsystem j. The probability is $P_3(k) = \Pr(CC_i(k) \cap (S_{j-1}(k) < w_i(k)(\rho_{J,i}(k) - \rho_i(k))))$, where $w_i, \rho_{J,i}$, ρ_i are the backward wave speed, the jam density, and the density of the first cell of subsystem j, respectively.
- The first cell of the downstream SCTM subsystem is congested (CC_i) and the sending function $S_{j-1}(k)$ is not less than its available space. In this case, an amount of vehicles which equals to the available space of the first cell of subsystem $j$will be loaded, The probability for this event is thus defined: $P_4(k) = \Pr(CC_i(k) \cap (S_{j-1}(k) \geqslant w_i(k)(\rho_{J,i}(k) - \rho_i(k))))$.

According to the definitions of probabilities of occurrence of the five modes, $FF_i(k)$ and $CC_i(k)$ are determined by the the traffic condition of the subsystem j at time k-1. To simplify the calculation, we assume $FF_i(k)$ and $CC_i(k)$ are independent of the events $(S_{j-1}(k) < Q_i(k))$, $(S_{j-1}(k) < w_i(k)(\rho_{J,i}(k) - \rho_i(k)))$, $(S_{j-1}(k) \geqslant Q_i(k))$, and $(S_{j-1}(k) \geqslant w_i(k)(\rho_{J,i}(k) - \rho_i(k)))$. Then the probabilities can be calculated as:

$$
\begin{aligned}
P_1(k) &= \left(P_{FF,j}(k) + P_{FC,j}(k)\right)\Pr\left(S_{j-1}(k) < Q_i(k)\right),\\
P_2(k) &= \left(P_{FF,j}(k) + P_{FC,j}(k)\right)\Pr\left(S_{j-1}(k) \geqslant Q_i(k)\right),\\
P_3(k) &= \left(P_{CC,j}(k) + P_{CF,j}(k)\right)\Pr\left(S_{j-1}(k) < w_i(k)\left(\rho_{J,i}(k) - \rho_i(k)\right)\right),\\
P_4(k) &= \left(P_{CC,j}(k) + P_{CF,j}(k)\right)\Pr\left(S_{j-1}(k) \geqslant w_i(k)\left(\rho_{J,i}(k) - \rho_i(k)\right)\right),
\end{aligned}
$$

with $\sum_y P_y(k) = 1$. We thus define the PDF for the traffic flow received by subsystem j, $R_j^a(k)$ as a finite mixture of the four probabilistic events:

$$
g_R\left(R_j^a(k)|\chi(k)\right) = \sum_y P_y(k) g_R\left(R_j^a(k)|\chi_y(k)\right), \tag{34}
$$

where $\chi(k) = \{\chi_y(k)\}$, $\chi_y(k) = (P_y(k), R_y(k))$. The set χ contains the four events defined previously, with P_y, $R_y(k)$, $y = 1, 2, 3, 4$, the probabilities and receiving flows of the four events. The mean and variance of the joint receiving flow (34) can be evaluated according to (16) and (17), respectively.

The interconnected SCTM approach calculates the flow propagation by pairing up two neighboring cells, which can be viewed as an extension of the approach used in the CTM. Consider the example depicted in Fig. 6. First, two cells are chosen to form a basic SCTM subsystem. By the basic SCTM subsystem, random traffic state (including the traffic density and the possible wavefront in terms of probabilities of occurrence of operational modes) of the segment is calculated. Then, the last cell of the upstream subsystem and the first cell of the downstream subsystem is paired up to calculate the flow across these two subsystems.

Fig. 7 depicts a flow chart for implementation of the SCTM for freeway traffic state estimation, to be more specific, the implementation of one SCTM subsystem in Fig. 4(b). As mentioned previously in the section, we first divide a freeway corridor into several segments with each of the segments modeled by one SCTM subsystem with appropriate cells. Then a

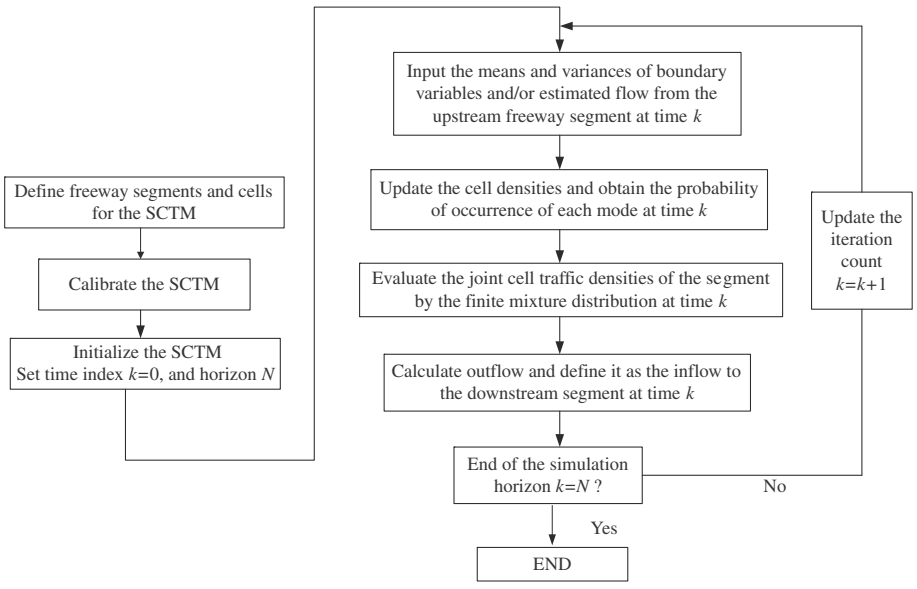

Fig. 7. The flow chart for implementation of the SCTM for a freeway segment.

calibration of the model is conducted, which gives the statistics of the boundary variables with respect to time. After initializing the SCTM, we are ready to run the simulation by specifying the boundary variables as inputs to the stretch SCTM system and the flow propagation between the neighboring SCTM subsystems.

4. Numerical example

To demonstrate the proposed method, we conduct the following numerical example. Consider a freeway segment consisting of four cells with neither on- nor off-ramp as depicted in Fig. 8. We assume that the first three cells of this freeway segment are of four lanes and the last cell consists of only 3 lanes. The cell length is set to be 100 m, and the time interval is $T = 5$ s.

It is assumed that the nominal flow–density relationships of all the four cells are characterized by triangular fundamental diagrams. The nominal fundamental diagrams of the first three cells and the last cell are shown in Fig. 9a and b, respectively. To illustrate the properties of the SCTM, the noise vector of the supply parameters $\{\xi^P(k), k \in N\}$ is as follows:

$$\xi^P(k) = \begin{bmatrix} v_f(k) \\ w_c(k) \\ \rho_J(k) \end{bmatrix} = \begin{bmatrix} v_f \\ w_c \\ \rho_J \end{bmatrix} + \begin{bmatrix} \xi_1(k) \\ \xi_2(k) \\ \xi_3(k) \end{bmatrix}, \tag{35}$$

where $\{\xi_i(k)\}$, $i = 1, 2, 3$ are mutually independent Normal distributed random sequences, and $v_f(k)$, $w_c(k)$ and $\rho_J(k)$ are respectively the vectors of the free-flow speed, the backward wave speed, and the jam density of all cells at time index k. The standard deviation of the uncertainties are assumed to be 10% of their nominal values. The sequences of $Q_M(k)$ and $\rho_c(k)$ can then be obtained by using the method given in Remark 3.1.

To test the build-up of congestion, we consider the following deterministic inflow profile:

$$q_u(k) = \begin{cases} 3000 \text{ vph}, & k \leqslant 50 \text{ time increment}; \\ 8000 \text{ vph}, & k \geqslant 50 \text{ time increment}. \end{cases} \tag{36}$$

This inflow profile yields two steady states: the first one is a free-flow state with $\rho = 50$ veh/km for all four cells while the second one is a congestion state with $\rho = 300$ veh/km for the first three cells and $\rho = 100$ veh/km for the last cell.

By applying the SCTM to this example, the means and SDs of the traffic densities on all four cells over time can be obtained as shown in Fig. 10. This figure plots the mean of the traffic density and the values of mean density plus and minus the SD. From the result, the traffic states during the low demand period (*i.e.*, time interval $[0, 50T]$) in the first three cells have relatively low variability. However, during the same time interval, there is a high variability of the traffic density in cell 4. In fact, the SD in this time interval increases as the flow moves to downstream cells. The gradual increase in SD and the high SD in cell 4 during this early period is due to the accumulation effect of the supply uncertainty. The downstream cells will therefore experience a higher level of uncertainties compared to the upstream cells. For the period with a higher probability of the occurrence of the congestion mode (*i.e.* $k > 50$), the variabilities of the traffic states, in the contrary, do not seem to increase as the flow moves downstream. On the other hand, in this case we can observe the propagation of the uncertainty in the reverse direction of the traffic flow. Under the congested condition, the bottleneck cell (cell 4) has a high probability to be congested due to the significant undersupply condition. Thus, the stochastic element of the backward wave becomes influential in which the uncertainty also propagates backward with the end of the queue (or backward wave).

For comparison, the Monte Carlo Simulation (MCS) with 5000 trials is also applied to the modified cell transmission model. The results in terms of the means and SDs of traffic densities are shown in Fig. 11. By comparing Figs. 10 and 11, we observe that the two methods provide similar results in terms of the mean traffic densities. However, the SDs of the densities in cells 1–3 for $k > 50$ as computed by the SCTM are significantly lower than those calculated from the MCS. The SDs from the MCS have smooth trends and transition particularly between the two steady states of the traffic condition (at $k = 50$). On the contrary, the SDs from the SCTM particularly in the last cell increases suddenly at the transition state.

Nevertheless, the trends of the SDs and means of the traffic densities in both cases are similar. It is not clear why the SD from the SCTM is lower than that from the MCS. However, it is noteworthy that the MCS is subject to the sampling error, which normally over-approximates the variance (or similarly SD). Various techniques for variance-reduction sampling have thus been proposed in the literature. On the other hand, the SCTM does not face this random sampling error. For the computational time, the SCTM only requires around 1% of the time taken by the MCS. In addition, the computer memory used by the SCTM is significantly less than that of the MCS.

The second test is set up to illustrate the propagation of SD over time and space. In this test, the same freeway corridor as shown in Fig. 8 is adopted but we assume that only the first cell admits uncertainties (and other three downstream cells have

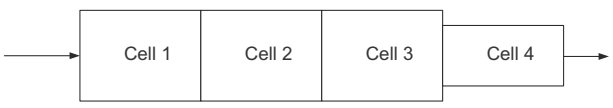

Fig. 8. Freeway segment consisting of four cells.

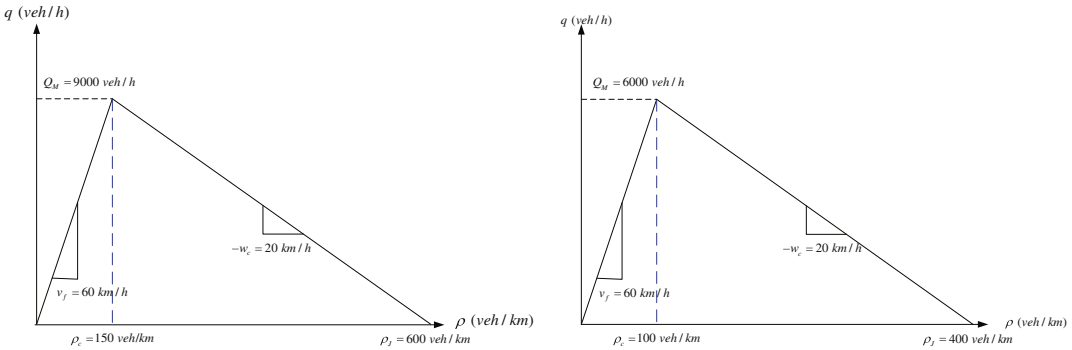

(a) Fundamental diagram of the first three cells (b) Fundamental diagram of the fourth cell

Fig. 9. The nominal fundamental diagrams.

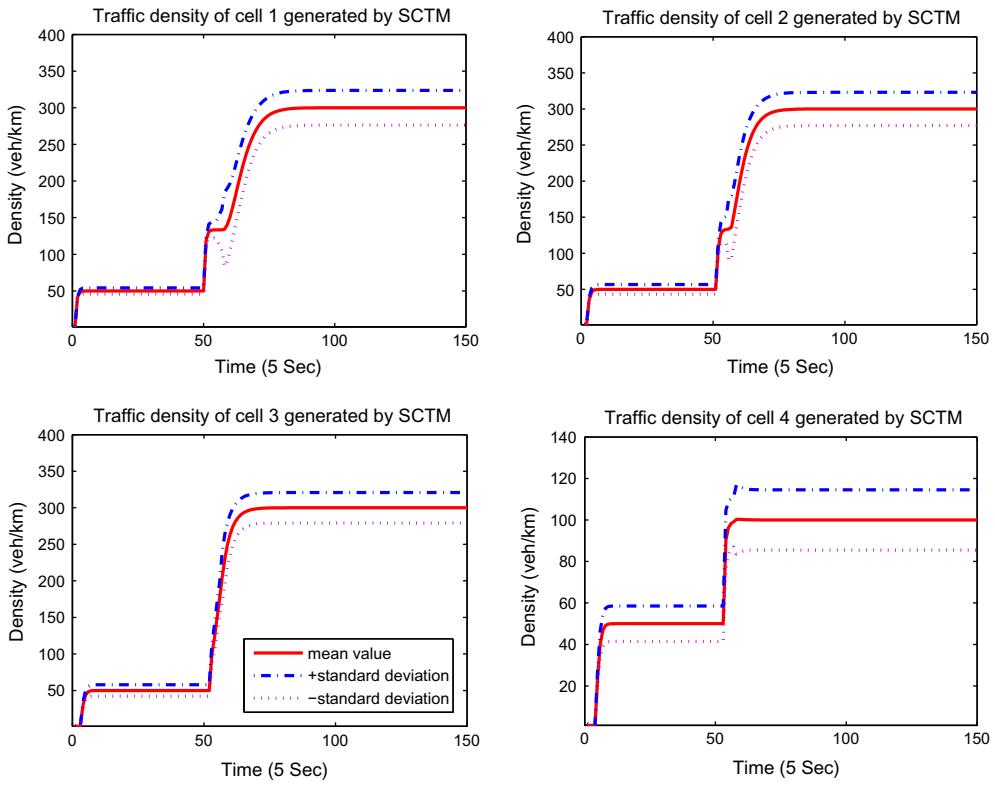

Fig. 10. Traffic density generated by the SCTM for the test case.

no supply uncertainties). The same inflow demand pattern as in (36) is adopted. The results are shown in Fig. 12. Despite the deterministic inflow pattern and supply characteristics of the last three cells, we can observe some uncertainties in the traffic densities in these three cells during the free flow and transition states. When the traffic is in the free-flow steady state (*i.e.*, flow moving downstream), the SD of traffic density in the first cell propagates downstream to the following three cells. The traffic densities during the transition period between the free flow and congested states also have certain levels of uncertainties (SD). This is due to the influence of the supply variability of the first cell which determines the time period that the downstream cells will become congested. However, once the freeway enters the state with a high probability of having congestion, the queue from the last cell builds up, spills backward and causes the last three cells to be in the definite congested state. The SDs of the last three cells during the congestion state are zero since there is no supply uncertainty and the cells are fully occupied by the vehicles.

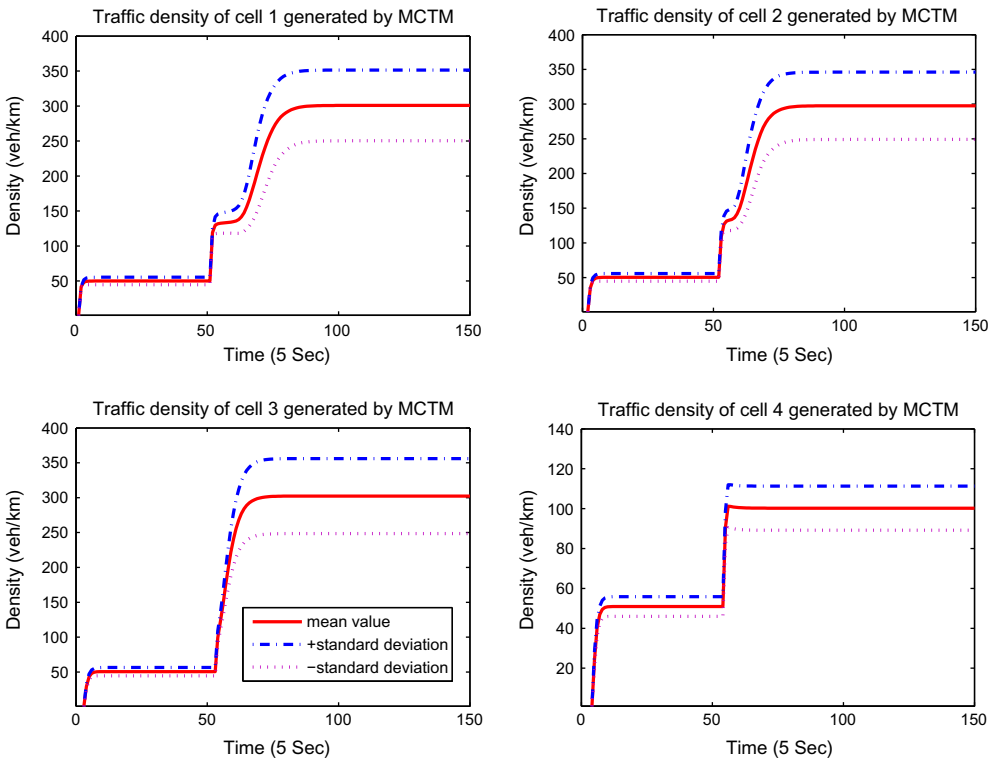

Fig. 11. Traffic density generated by the Monte Carlo Simulation of MCTM.

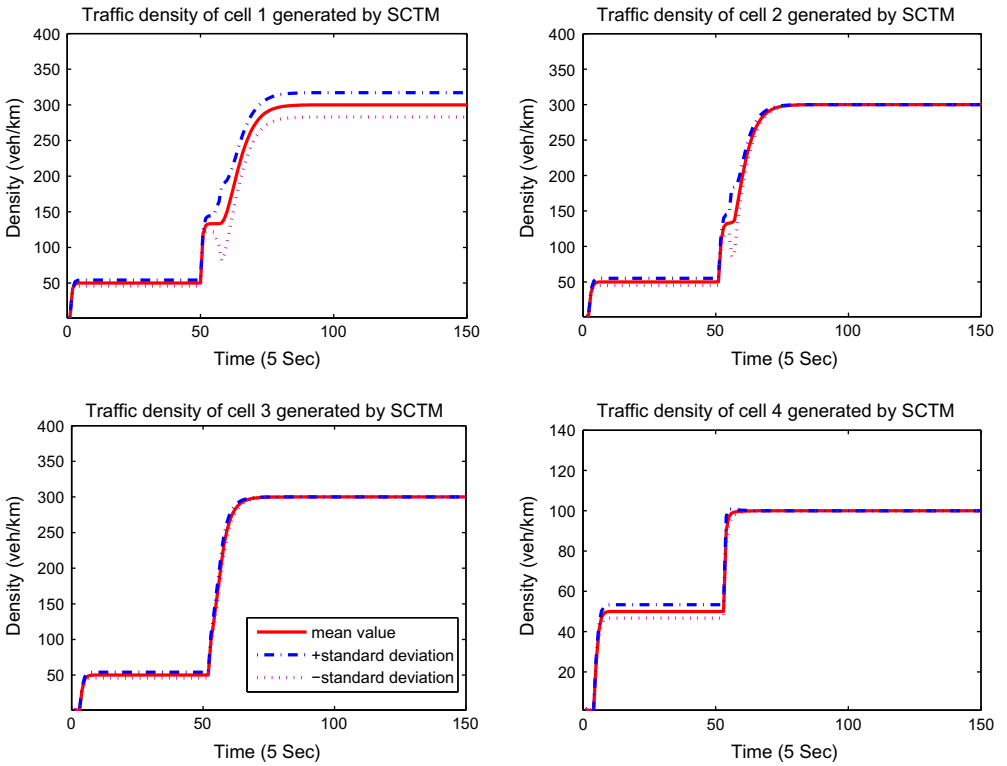

Fig. 12. Propagation of SD of the traffic density.

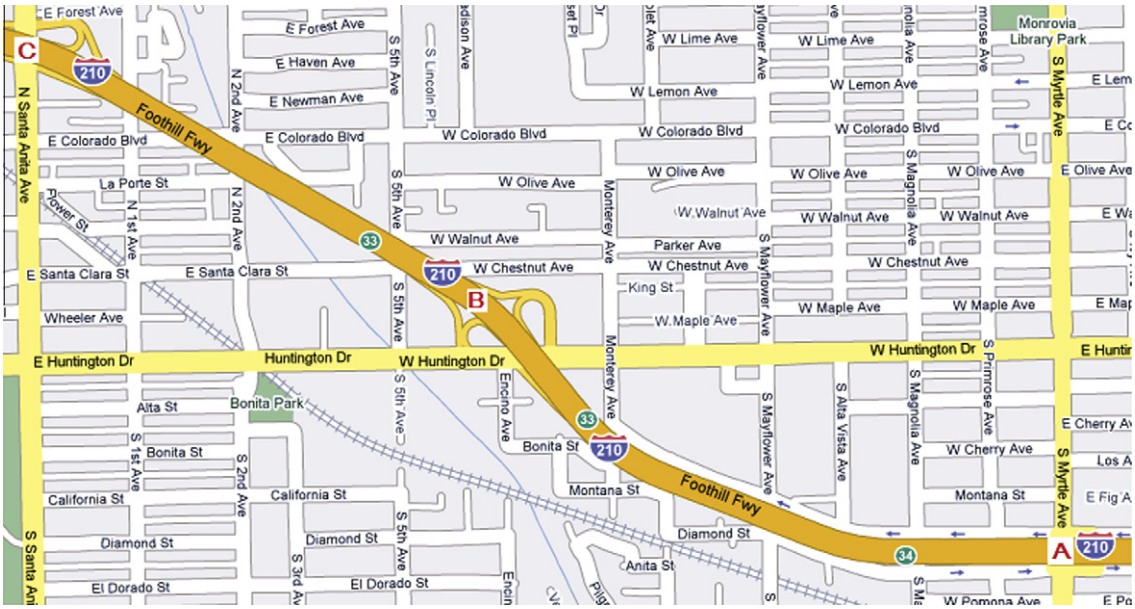

Fig. 13. Map of the test site. *Source*: Google map.

5. An empirical study

In this section, we will validate the SCTM by two scenarios with empirical traffic data:

- The first scenario is to test the proposed model against the supply uncertainty, i.e. only uncertain supply functions are considered. In this case, the demand pattern is chosen from a particular day. The utilized traffic flow data of 24 h were collected on April 22, 2008 from the Performance measurement system (PeMS).[4] In this study, we will compare the performance of the SCTM against those obtained from the MCTM and MCS of the MCTM to validate the proposed model.
- The second scenario is to validate the SCTM against both demand and supply uncertainties. In this case, the demand pattern is obtained from a statistical analysis of the historical data. Traffic flow data of 7 h (4:00 am–11:00 am) collected on Tuesday, Wednesday and Thursday of April 2008 and April 2009 from the PeMS is utilized in this test.

5.1. Test site description and model parameters calibration

The region of interest is a section of Interstate 210 West, approximately two miles in length, as shown in Fig. 13. This section, located in Los Angeles, stretches from S Myrtle Ave (A) through W. Huntington Dr(B) to N Santa Anita Ave(C), and contains 2 on-ramps and 2 off-ramps. The section is instrumented with single-loop inductance detectors, which are embedded in the pavement along the mainline, HOV lane, on-ramps, and off-ramps. Typically, on I-210, mainline loop detectors are situated slightly upstream of on-ramp merge points. This segment of freeway is chosen here for the following reasons:

1. The high level of recurrent congestion within the section can be observed in the early morning period (6 am–10 am).
2. The segment possesses necessary infrastructure and traffic detectors embedded in the on-ramps and mainline lanes for data collection.

Fig. 14 depicts the test section partitioned into four cells with lengths range from 0.45 to 0.5 miles. The green points along the freeway segment denote where and how many loop detectors are installed. Each loop detector group is assigned a signature of six digital numbers. q_u denotes the inflow profile of the freeway segment while q_o is the outflow profile. r_1 and r_2 denote the two on-ramps while f_1 and f_2 denote the two off-ramps. q_m denotes the flow detected by the detector installed on the boundary between cells 2 and 3. Each loop detector gives volume (veh/time step) and occupancy measurements every 30 s. Densities could then be computed for each lane using the occupancy divided by the g-factor, where the g-factor is the effective vehicle length, in miles, for the detector. A necessary condition for the numerical stability of CTM is that vehicles

[4] The Freeway Performance Measurement System (PeMS: http://pems.eecs.berkeley.edu/) is conducted by the Department of Electrical Engineering and Computer Sciences at the University of California, at Berkeley, with the cooperation of the California Department of Transportation, California Partners for Advanced Transit and Highways, and Berkeley Transportation Systems.

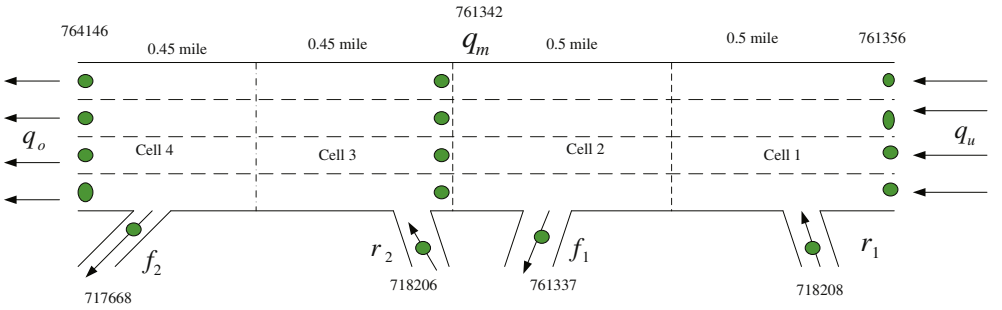

Fig. 14. A section of I210-W divided into four cells and its detector configuration.

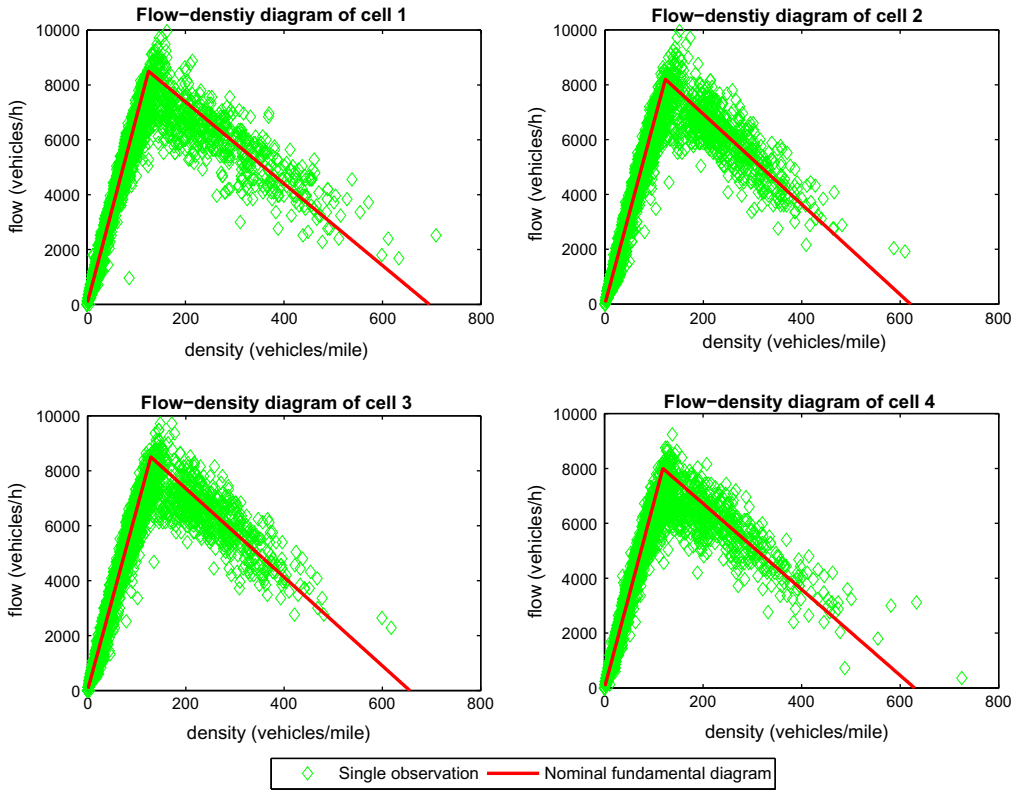

Fig. 15. The fundamental diagrams of the four cells calibrated from the traffic flow data collected on April 22, 2008.

traveling at the maximum speed may not cross multiple cells in one time step, that is, $v_{f,i} \cdot T_s \leqslant l_i$. This in conjunction with the aforementioned cell lengths prohibits a simulation time step as large as 30 s. Thus a *zero*th-order interpolation is applied to the PeMS data to yield data with $T_s = 5$ s in order to make $v_{f,i} \cdot T_s \leqslant l_i$ holds for almost all the time.[5] As it was mentioned in Muñoz et al. (2003), one difficulty in selecting a test section is that it is rare for all the loop detectors in a section to be functioning properly at the same time. In the cases where detectors were not functional, the data was corrected using information from neighboring sensors or data from similar days. The interpolated, filtered, and corrected data sets were used as simulation inputs. As shown in Fig. 15, by assuming that all the parameters must satisfy the triangular fundamental relationship and using the least square method, calibration was conducted for the four cells. Calibration results are listed in Table 1. The notations with hats denote the mean values of the parameters. As for example, $\hat{v}_f$ denotes the mean values of free-flow speeds for the four cells. The notations σ with the mean notations as subscripts denote the standard deviations of the

[5] In fact, the FIFO condition, *i.e.*, $v_f T_s \leqslant l_i$, proposed in the CTM to ensure numerical stability, can not be always satisfied in our formulation, since the free-flow speed v_f can be anything along its distribution. The concept we used here is the probabilistic FIFO which can be roughly defined as $Pr(v_{f,i} \cdot T_s \leqslant l_i) \geqslant \chi$, where χ is a positive real number which satisfies $1 - \epsilon < \chi \leqslant 1$ for a small real number $\epsilon > 0$.

Table 1
Calibration results of the four cells against the traffic flow data collected on April 22, 2008.

	$\hat{v}_f$	$\sigma_{\hat{v}_f}$	$\hat{w}_c$	$\sigma_{\hat{w}_c}$	$\hat{\rho}_c$	$\hat{\rho}_J$	$\sigma_{\hat{\rho}_J}$	$\widehat{Q}_m$	$\sigma_{\widehat{Q}_m}$
Cell 1	64.2	5.5	15.3	4.4	132.4	686.2	172.8	8500	725.6
Cell 2	63.8	5.7	19.3	5.4	133.3	573.0	133.5	8500	764.1
Cell 3	63.2	5.5	16.6	4.9	134.6	645.4	164.0	8500	746.2
Cell 4	63.2	4.9	16.2	4.9	126.5	619.6	162.1	8000	753.4

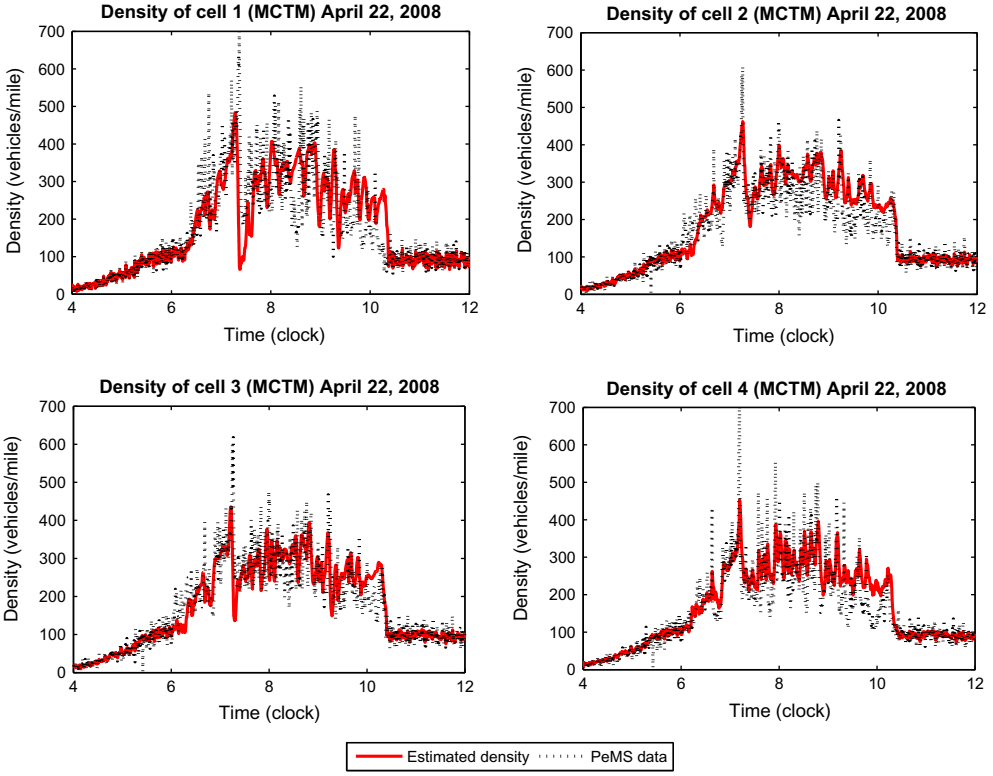

Fig. 16. Measured densities and the MCTM's estimated densities for a segment of I-210W on April 22, 2008.

corresponding parameters. Compared with previous studies, such as Muñoz et al. (2003), we can verify that our calibration results are reasonable.

5.2. Test results against the supply uncertainty

In this subsection, three models, namely the MCTM, the Monte Carlo Simulation of MCTM and the SCTM, are used to simulate the traffic flow pattern for the calibrated section, between 4 am and 12 am, during some of which the morning rush-hour congestion normally occurs. This time interval is chosen also for the reason that all the five modes would be active during this time interval. First, the MCTM is applied to the test site with the PeMS data and the calibration results. The measured and simulated mainline densities are depicted in Fig. 16. As it was a normal day with a good calibration, the MCTM gives a quite satisfactory result. However, as we can see from the figure, good results are obtained for cells 1 and 3 only under the free-flow condition. The congestion states for these two cells are not well estimated by the MCTM. This may be due to the fact that congestion state introduces more supply uncertainties to our fundamental diagram than the free-flow state, as demonstrated in Fig. 15. To verify this, the Monte Carlo Simulation (MCS) of MCTM is conducted. By assuming the uncertainties obey normal distribution with means and standard deviations given in Table 1, the MCS of MCTM is conducted with 500 samples. The mean values of the simulated traffic densities are plotted against the measured traffic densities in Fig. 17. As expected, some improvement is achieved by the MCS of MCTM, but not very significant. Fig. 18[6] depicts the mean values of

[6] In the figures involving SDs in this section, we plot the PEMS raw data every 15 min to reduce the resolution to make the figure clearer and more readable, while the simulated results are plotted every 5 min.

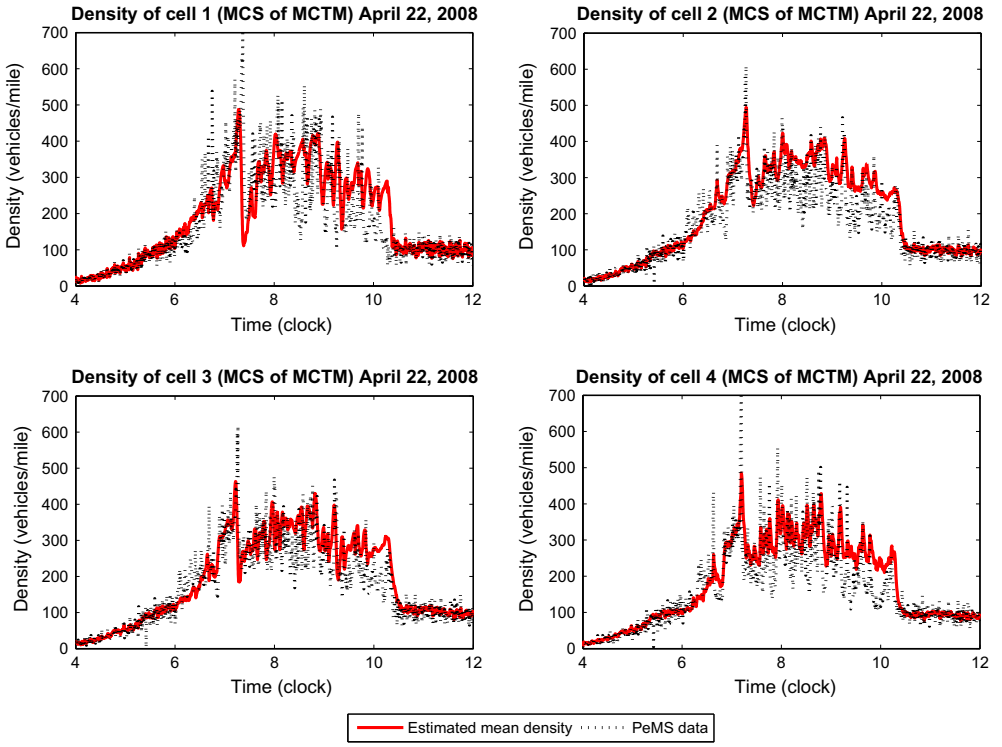

Fig. 17. Measured densities, simulated mean densities obtained by the MCS of MCTM for a segment of I-210W on April 22, 2008.

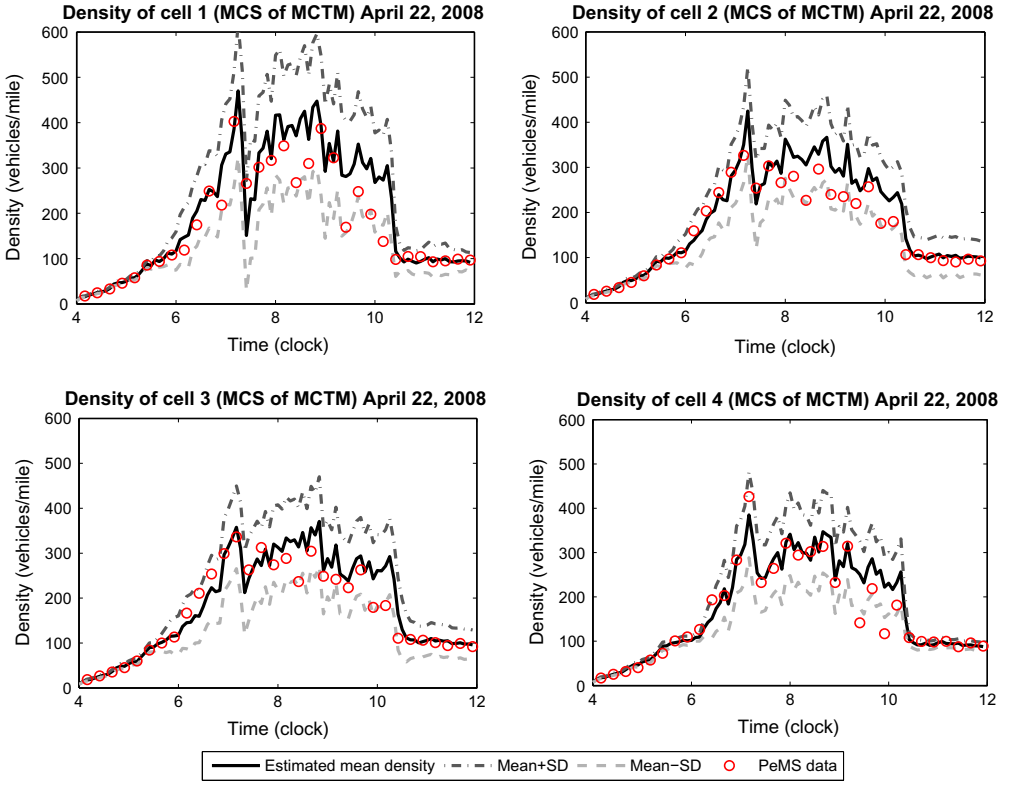

Fig. 18. Measured densities, simulated mean densities, and the 68% confidence interval obtained by the MCS of MCTM for a segment of I-210W on April 22, 2008.

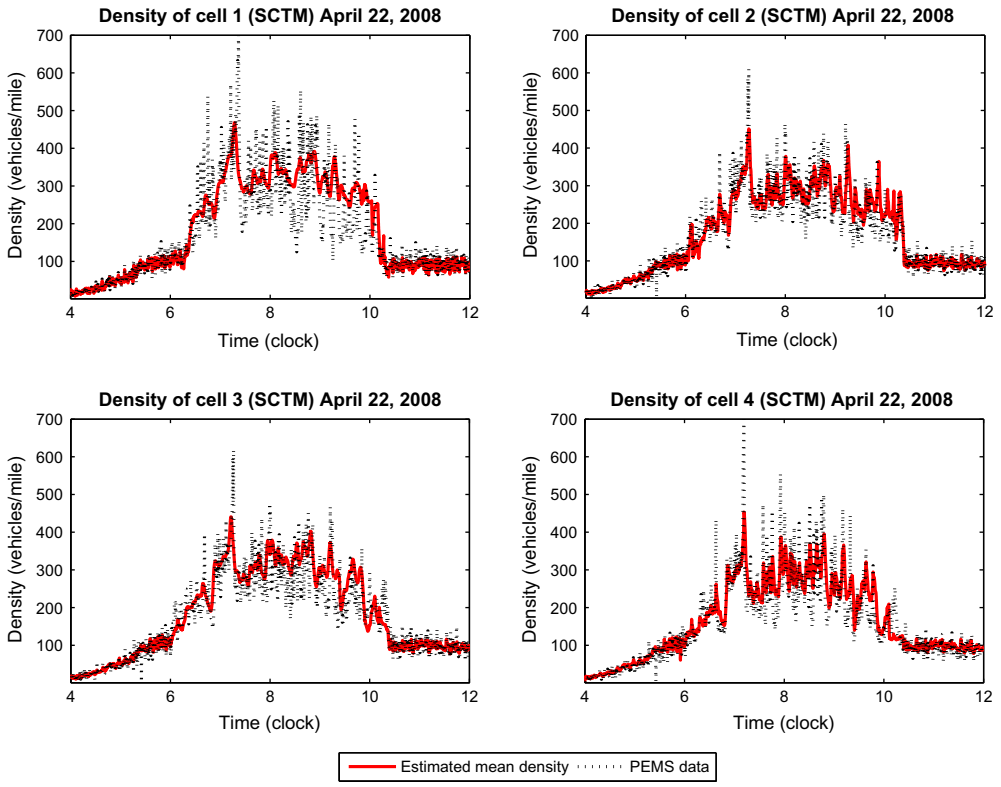

Fig. 19. Measured densities and estimated mean densities by the SCTM for a segment of I-210W on April 22, 2008.

the simulated densities and its 68% confidence interval, *i.e.* $[\bar{\rho} - \sigma_{\rho}, \bar{\rho} + \sigma_{\rho}]$, generated by the MCS of MCTM against the measured traffic densities. Almost all the measured traffic densities including the sharp impulse points fall in this interval. We can conclude from Fig. 18 that the MCS of MCTM with 500 samples over estimates the means and variances of the traffic densities (the 68% confidence interval covers almost all the data), which is consistent with our previous simulation results. Regardless of the accuracy, this MCS of MCTM is already computational and memory demanding.

Next, we apply the interconnected SCTM approach to estimate the traffic state. We divide the segment into two interconnected subsystems with each subsystem having two cells. The results are shown in Figs. 19–21. The mean values of the simulated traffic densities generated by the SCTM are plotted against the measured traffic densities in Fig. 19. The figure demonstrates that the SCTM outperforms the other two techniques, *i.e.* the MCTM, and the MCS of MCTM in this test example. By comparing Fig. 19 with Fig. 17, the SCTM produces more accurate estimated mean values than the MCS of MCTM. The mean values generated by the SCTM follow the measured data closely but in a smoother way, especially in the morning peak. Fig. 20 depicts the mean values of the simulated densities and its 68% confidence interval generated by the SCTM against the measured traffic densities. One can conclude from this figure that the SCTM produces more reasonable variances when compared with the MCS of MCTM. About 60% of the measured traffic density data falls in the interval excluding almost all the sharp impulse points. All these sharp impulse points are taken as noise in the PeMS 30-s data. To counteract the noise, a 1st-order Butterworth low-pass filter was applied to the data using a zero-phase forward-and-reverse filtering technique, see Muñoz et al. (2003). From this example, the SCTM is found to be adaptive to the noise. The probability distributions for all five modes over time are depicted in Fig. 21. At the beginning, *i.e.*, from 4 am to 5:30 am, the FF mode dominates the stochastic traffic states. After the traffic densities increase to the critical densities, the transient modes become active. The CC mode dominates the states after the transient modes. Due to the fast varying measured traffic data, all the three transient modes are active, without one dominating the simulation. From 10:30 am onward, the measured traffic densities are sliding near to the critical densities. The FF mode and its transient modes become active again.

5.2.1. Reproducing missing data

It is assumed that the upstream and downstream mainline data (q_u, q_d), as well as the ramp flow data, are known, whereas the middle density, ρ_m, is considered to be "missing", which must be estimated. The purpose of this test is to determine whether the models can accurately reproduce ρ_m. By applying the PeMS data to the SCTM, the following simulation result is obtained. The flow data, q_m, which is assumed to be missing is reproduced by the SCTM and plotted against the measured data in Fig. 22. From the results, the missing flow and density data is reproduced in a satisfactory manner.

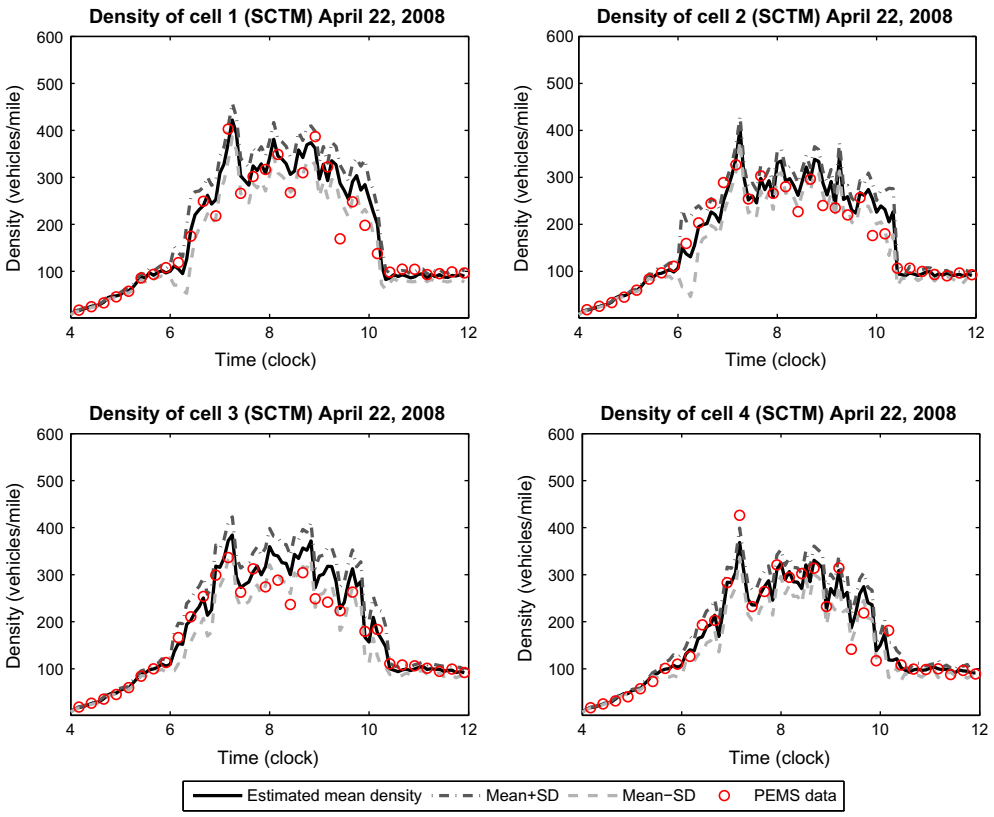

Fig. 20. Measured densities, estimated mean densities and the 68% confidence interval by the SCTM for a segment of I-210W on April 22, 2008.

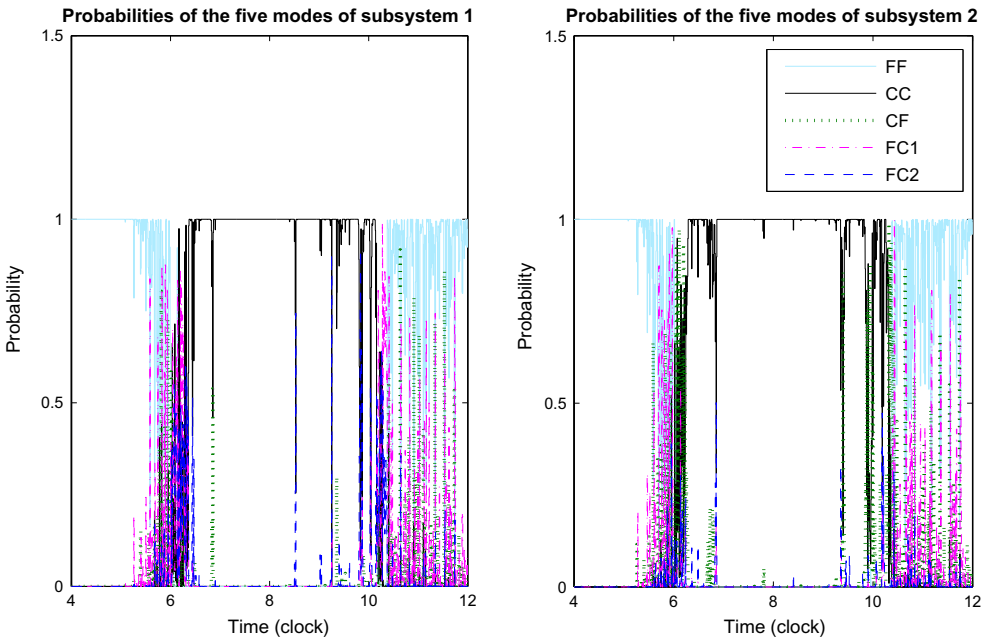

Fig. 21. Probability distributions of different modes in the SCTM approach over time.

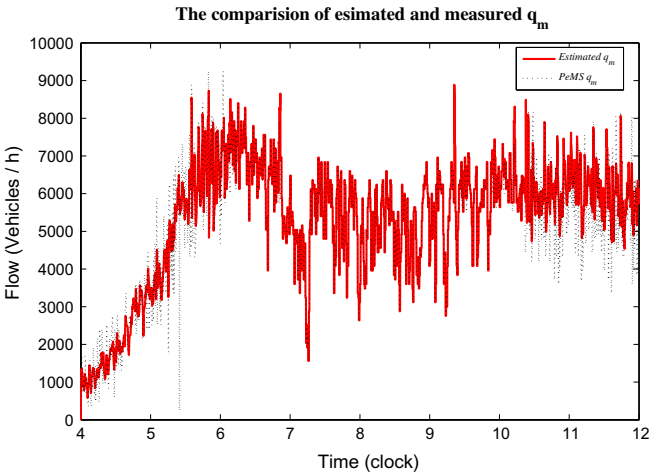

Fig. 22. The measured "missing" flow q_m and its estimated value.

Table 2
Calibration results of the four cells against the historical data over the selected days.

	$\hat{v}_f$	$\sigma_{\hat{v}_f}$	$\hat{w}_c$	$\sigma_{\hat{w}_c}$	$\hat{\rho}_c$	$\sigma_{\hat{\rho}_c}$	$\hat{\rho}_J$	$\sigma_{\hat{\rho}_J}$	$\widehat{Q}_m$	$\sigma_{\widehat{Q}_m}$
Cell 1	63.6	8.95	25.72	9.12	149.36	21	518.68	149.83	9500	1336.5
Cell 2	62.46	6.69	21.69	7.16	137.68	14.75	534.22	146.80	8600	921.46
Cell 3	62.46	6.69	23.25	7.87	140.88	15.09	519.30	144.67	8800	942.89
Cell 4	63.29	7.01	20.30	6.31	127.97	14.17	526.96	137.20	8100	897.06

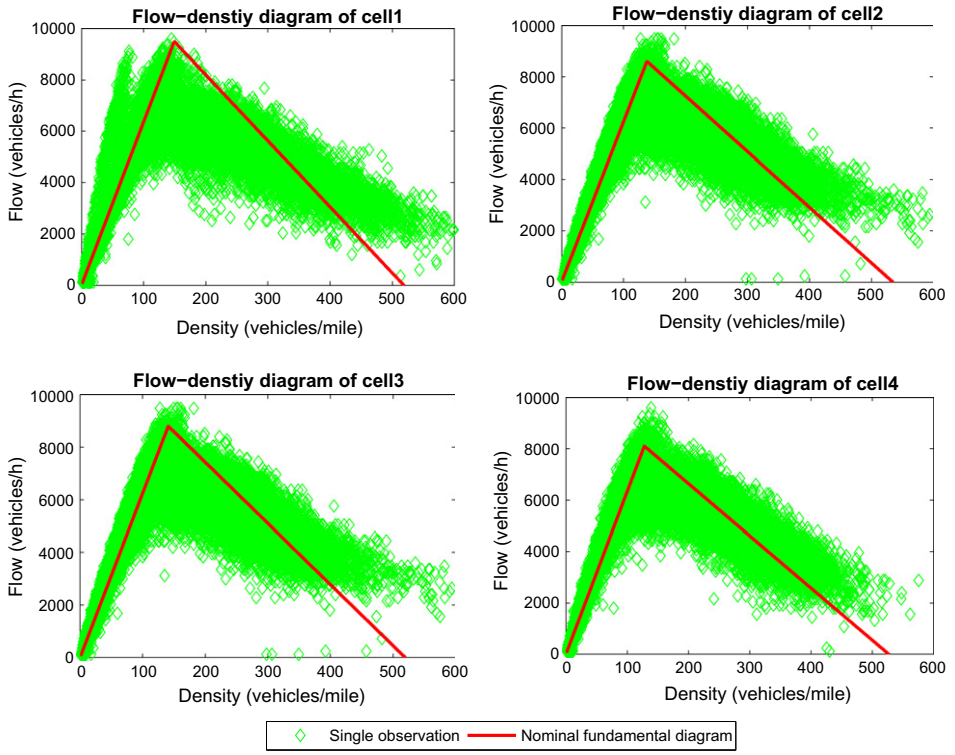

Fig. 23. The fundamental diagrams of the four cells calibrated from the historical data over the selected days.

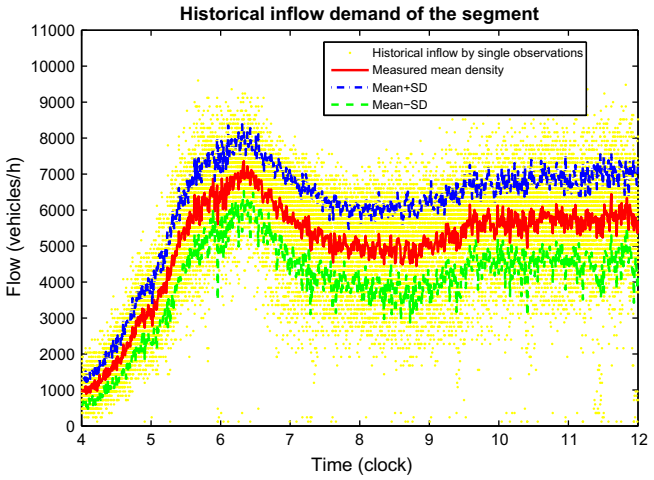

Fig. 24. A demonstration of the demand uncertainty.

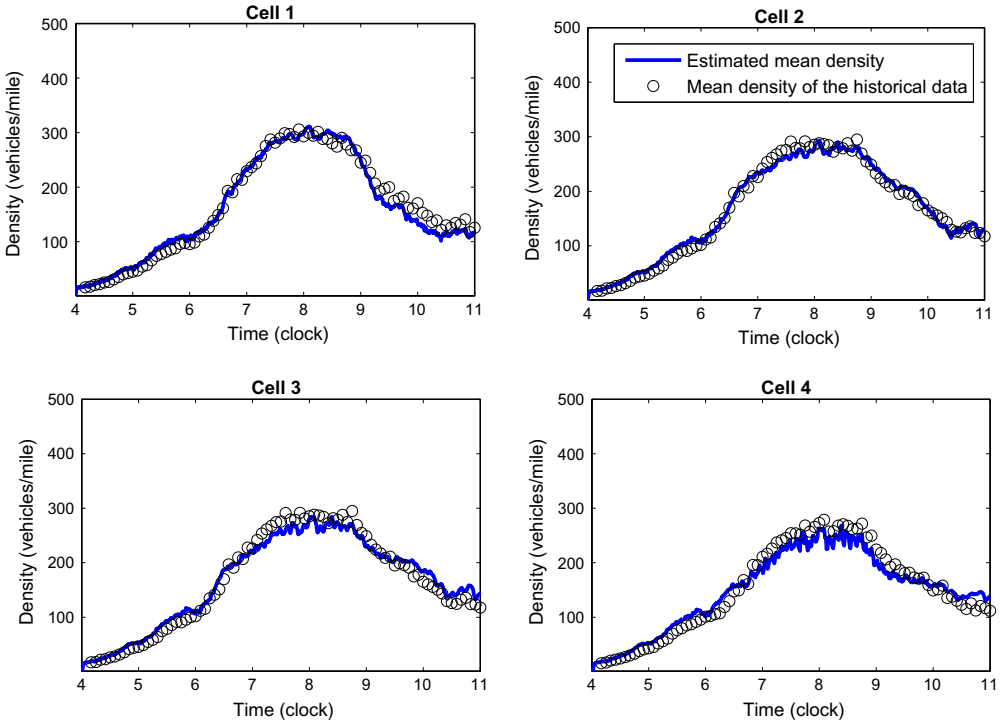

Fig. 25. The estimated mean densities against the historical mean densities.

5.3. Test results against both demand and supply uncertainties

This test aims to validate the SCTM against both demand and supply uncertainties. We use the traffic flow data of 7 h (4:00 am–11:00 am) collected on Tuesday, Wednesday and Thursday of April 2008 and April 2009 from the PeMS in this test. The calibration of the stochastic triangular fundamental diagram is conducted for the four cells by using the historical data over the selected days. The results are shown in Table 2 and Fig. 23. As illustrated in Table 2 and Fig. 23, the supply functions admit significant uncertainties. The calibrated variances of the supply functions are lager than those shown in Table 1 in the previous test. Statistical analysis on the collected traffic data is also conducted for the demand side. The observed raw data of the inflow to the upstream of the segment, its mean and standard deviation with respect to time are depicted in Fig. 24. From

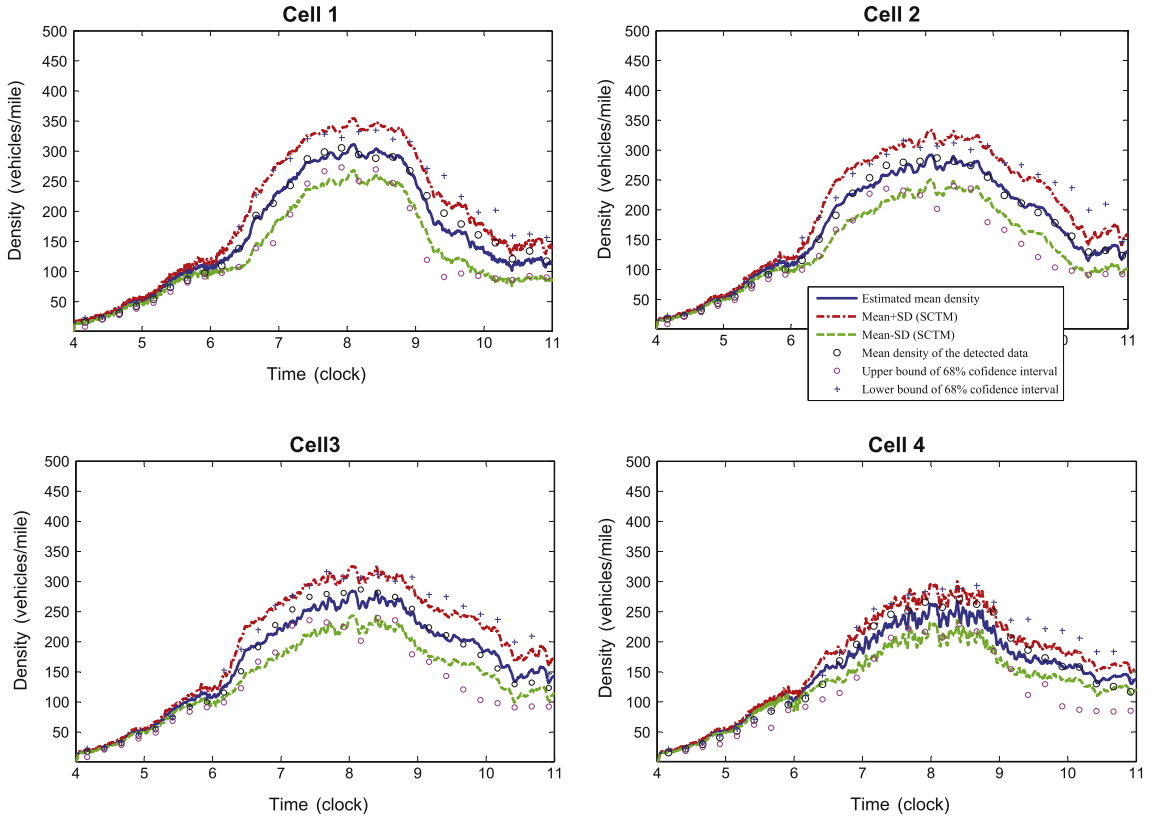

Fig. 26. The estimated mean densities and the 68% confidence against the historical data over the selected days.

Table 3
The mean absolute percent errors of the four cells.

	Cell 1	Cell 2	Cell 3	Cell 4	Average
MAPE	7.47 %	6.12 %	7.77 %	10.2 %	7.89 %

this figure, we can observe that the inflow profile admits significant uncertainty. In a word, both the demand[7] and supply sides admit significant uncertainties.

We input the calibrated means and variances to simulate the SCTM. The estimated traffic densities are depicted against the historical data over the selected days in Figs. 25 and 26. The corresponding mean absolute percent error (MAPE) between estimated mean traffic densities and the observed mean traffic densities of the four cells are reported in Table 3. It can be seen from Fig. 25 that the SCTM produces an accurate estimation of mean traffic densities. The corresponding average MAPE of the four cells is about 7.9% as indicated in Table 3. We can observed from Fig. 26 that the estimated variances are smaller than the observed ones especially when it approaches to the tail end of the simulation horizon. Besides the error introduced by the LWR model (and its discretized version—the CTM) to approximate the traffic dynamics, this under-estimation of variance may be due to the following two reasons:

- First, as illustrated in the numerical example, the SCTM itself under estimates the variance of traffic density. This may be caused by the finite mixture (Gaussian sum) approach we utilized to approximate any possible random distribution of the traffic density.
- The second reason would be the noises and errors introduced by the data detection and conversion of PeMS. The overall average error is reported to be about 16% (Chen, 2003,).

6. Conclusions

In this paper, a stochastic cell transmission model (SCTM) is proposed for simulating the traffic density of a freeway section under stochastic demand and supply. The uncertainty terms are assumed to be wide-sense stationary, second-order processes

[7] As we utilize the measured traffic flow data, the demand here is the statistics of historical detected inflow(s) to the segment.

consisting of uncorrelated random vectors with known means and variances. The stochasticities of the sending and receiving functions in the SCTM are governed by the random parameters of the fundamental flow–density diagrams, including the capacities, backward wave speeds, and the free-flow speeds. The model also permits random demand inflow patterns. The switching mode model of the CTM is adopted to avoid the nonlinearity of the original CTM caused by the "min" operator. The SCTM is formulated as a class of discrete time stochastic bilinear systems. A set of probabilistic switching conditions between different traffic modes for the SCTM is introduced. The paper then provides analytical approximations of the means and SDs of the traffic densities. Numerical examples and an empirical study are carried out to illustrate the advantages of the SCTM over the Monte Carlo Simulation approach in terms of computation time and memory requirement. The illustration of the propagation of uncertainties of traffic states over time and space is also provided. However, there are some discrepancies between the SDs of traffic densities from the SCTM and Monte Carlo Simulation which may be due to the sampling error of the Monte Carlo Simulation. Empirical results from I-210W freeway case in Southern California conclude that the MCS of MCTM overestimates the SDs of the traffic densities while the SCTM underestimates the SDs a bit. The empirical study confirms that the SCTM performs well for all traffic conditions ranging from light to very dense traffic conditions. This is an advantage of the proposed model over the previous proposed macroscopic stochastic dynamic traffic models, (*e.g.* Boel and Mihaylova, 2006; Kim and Zhang, 2008). The empirical study also reveals that the SCTM outperforms the MCTM, and the MCS of MCTM.

For the surveillance purpose, the SCTM can be utilized to provide a short-term prediction using the historical and on-line data of travel demand and traffic state. The prediction (in terms of travel time and traffic state) under the SCTM considers both demand and supply uncertainties in the future time step. This allows traffic operators to monitor and devise robust control strategies for freeways. Sumalee et al. (submitted for publication) utilizes the SCTM model for the short-term prediction of the stochastic travel time. For the dynamic traffic assignment and control, Zhong et al. (submitted for publication) extends the SCTM framework to model traffic flows on a general network. The key operational benefit of the SCTM for traffic assignment purpose, as discussed in Zhong et al. (submitted for publication), is the potential continuity of the delay operator which is not the case for the deterministic CTM (due to the potential blocking back condition of an arterial). This is due to the introduction of the stochastic delay in the SCTM which can also be considered as a better paradigm for a long-term traffic prediction. Note that there are several assumptions which were made to simplify the construction and analysis of the SCTM. Two key future research issues are envisaged including (i) introduction of spatial and temporal correlations of the stochastic fundamental diagrams and (ii) investigation of theoretical relationship between the SCTM and the LWR model with stochastic components. Apart from these two fundamental research issues, the study of the existence and property of the dynamic user equilibrium (DUE) solution based on the SCTM framework should also be carried out.

Acknowledgments

This research is jointly sponsored by the project funded by University Research Grant A-PH65 from the Hong Kong Polytechnic University, and the project supported by the Research Grants Council of the Hong Kong Special Administration Region under Grant Project No. PolyU 5271/08E. The authors would like to thank Dr. Gabriel Gomes, Dr. Lyudmila Mihaylova, and the two anonymous referees for their constructive comments and suggestions, which led to improvements in the study. Special thanks should also go to the Freeway Performance Measurement (PeMS) Project which provides the data in the empirical study.

Appendix A. A small analytical numerical example

In this Appendix, we give a small analytical numerical example to illustrate the implementation of the SCTM. We consider a freeway segment consisting of two cells without on- nor off-ramp. The simulation time step is 5 s. The two cells are 100 m long. We assume that the two cells admit the same nominal fundamental diagram as depicted in Fig. 9(b). The SDs of the parameters are assumed to be 10% of their nominal values. The SCTM has an constant inflow rate of 5000 veh/h. Then the system matrices for the FF mode, i.e. Eq. (19), are given as

$$A_1 = \begin{bmatrix} -0.0139 & 0 \\ 0.0139 & 0 \end{bmatrix}, \quad A_2 = \begin{bmatrix} 0 & 0 \\ 0 & -0.0139 \end{bmatrix}, \quad B = \begin{bmatrix} 0.0139 & 0 \\ 0 & 0 \end{bmatrix}. \tag{37}$$

The system matrices for the CC mode, i.e. Eq. (20), are obtained as

$$A_1 = \begin{bmatrix} -0.0139 & 0 \\ 0 & 0 \end{bmatrix}, \quad A_2 = \begin{bmatrix} 0 & 0.0139 \\ 0 & -0.0139 \end{bmatrix}, \quad B_1 = -A_1, \quad B_2 = -A_2, \quad B = \begin{bmatrix} 0 & 0 \\ 0 & -0.0139 \end{bmatrix}. \tag{38}$$

The system matrices for the CF mode, i.e. Eq. (21), are obtained as

$$A_1 = \begin{bmatrix} -0.0139 & 0 \\ 0 & 0 \end{bmatrix}, \quad A_2 = \begin{bmatrix} 0 & 0 \\ 0 & -0.0139 \end{bmatrix}, \quad B_0 = \begin{bmatrix} 0 & -0.0139 \\ 0 & 0.0139 \end{bmatrix}, \quad B_1 = \begin{bmatrix} 0.0139 & 0 \\ 0 & 0 \end{bmatrix}, \quad B_2 = 0. \tag{39}$$

The system matrices for the FC1 mode, i.e. Eq. (22), are:

$$A_1 = \begin{bmatrix} -0.0139 & 0 \\ 0.0139 & 0 \end{bmatrix}, \quad B = \begin{bmatrix} 0.0139 & 0 \\ 0 & -0.0139 \end{bmatrix}. \tag{40}$$

The system matrices for the FC2 mode, i.e. Eq. (23), are:

$$A_2 = \begin{bmatrix} 0 & 0.0139 \\ 0 & -0.0139 \end{bmatrix}, \quad B_2 = \begin{bmatrix} 0 & -0.0139 \\ 0 & 0.0139 \end{bmatrix}, \quad B = \begin{bmatrix} 0.0139 & 0 \\ 0 & -0.0139 \end{bmatrix}. \tag{41}$$

Other matrices which are not specified here are null matrices. To illustrate the evolution, the mean traffic densities of the two cells at time step $k = 30$ equal to 83.2870 and 83.0789 veh/km are obtained from the SCTM. The corresponding SDs are 10.3376 and 15.2070 veh/km for the two cells, respectively. The auto-correlation matrix is $Q(30) = \begin{pmatrix} 7043.6 & 6876.4 \\ 6876.4 & 7133.4 \end{pmatrix}$. Then we can obtain the probabilities of occurrence of the five modes as $P_{FF}(30) = 0.7225$, $P_{CC}(30) = 0.0217$, $P_{CF}(30) = 0.1011$, $P_{FC1}(30) = 0.1278$, and $P_{FC2}(30) = 0.0270$ according to the method proposed in Section 3.3. The means and auto-correlation matrices of traffic densities of the five modes at $k = 31$ can be calculated according to the dynamics proposed in Section 3.4 and the corresponding evaluations developed in Section 3.5. For example, the mean and auto-correlation matrix of the FF mode are thus calculated:

$$\rho_{FF}(31) = (I + 60A_1 + 60A_2)\begin{pmatrix} 83.2870 \\ 83.0789 \end{pmatrix} + B\begin{pmatrix} 5000 \\ 0 \end{pmatrix} = \begin{pmatrix} 83.3256 \\ 83.2523 \end{pmatrix},$$

$$Q_{FF}(31) = (I + 60A_1 + 60A_2)Q(30)(I + 60A_1 + 60A_2)^T + 36A_1Q(30)A_1^T + 36A_2Q(30)A_2^T + G_1(30) + G_1^T(30) + B\begin{pmatrix} 5000 \\ 0 \end{pmatrix}\begin{pmatrix} 5000 \\ 0 \end{pmatrix}^T B^T = \begin{pmatrix} 6995.0 & 6901.8 \\ 6901.8 & 7098.1 \end{pmatrix},$$

where $G_1(30) = \left(I \times \begin{pmatrix} 83.2870 \\ 83.0789 \end{pmatrix}[5000\ 0] + (A_1 + A_2) \times \begin{pmatrix} 83.2870 \\ 83.0789 \end{pmatrix}[60 \times 5000\ 0]\right)B^T = \begin{pmatrix} 964 & 0 \\ 5781.4 & 0 \end{pmatrix}$. The means and auto-correlation matrices of other modes can be similarly obtained, we list them here as

$$\rho_{CC} = \begin{pmatrix} 83.2292 \\ 87.7792 \end{pmatrix}, \quad Q_{CC} = \begin{pmatrix} 7388 & 7127.4 \\ 7127.4 & 8028.2 \end{pmatrix}, \quad \rho_{CF} = \begin{pmatrix} 87.9295 \\ 97.1798 \end{pmatrix}, \quad Q_{CF} = \begin{pmatrix} 8059 & 8470.3 \\ 8470.3 & 9569.3 \end{pmatrix},$$

$$\rho_{FC1} = \begin{pmatrix} 83.3256 \\ 69.1514 \end{pmatrix}, \quad Q_{FC1} = \begin{pmatrix} 6995 & 5720.8 \\ 5720.8 & 5064.6 \end{pmatrix}, \quad \rho_{FC2} = \begin{pmatrix} 64.6978 \\ 87.7792 \end{pmatrix}, \quad Q_{FC2} = \begin{pmatrix} 4489 & 5492.1 \\ 5492.1 & 8028.2 \end{pmatrix}.$$

By substituting these means and auto-correlation matrices into Eqs. (16) and (17), we obtain the means of the joint traffic densities for $k = 31$ as

$$\mu(31) = \sum_s P_s(30)\rho_s(31) = \begin{pmatrix} 83.2870 \\ 83.0789 \end{pmatrix},$$

$$diag\{Var(\bar{\rho}(31)|\theta(31))\} = diag\left\{\sum_s P_s(30)Q_s(31) - \mu(31)\mu^T(31)\right\} = \begin{pmatrix} 106.865 & 0 \\ 0 & 231.2515 \end{pmatrix}.$$

The corresponding SDs are 10.3376 and 15.2070 veh/km.

References

Boel, R., Mihaylova, L., 2006. A compositional stochastic model for real time freeway traffic simulation. Transportation Research Part B 40 (4), 319–334.

Chen, C., Jia, Z., Varaiya, P., 2001. Causes and cures of highway congestion. IEEE Control Systems Magazine 21 (6), 26–33.

Chen, C., 2003. Freeway Performance Measurement System (PeMS). Ph.D. Dissertation, University of California, Berkeley.

Chen, C., Kwon, J., Rice. J., Skabardonis, A., Varaiya, P., 2003. Detecting Errors and Imputing Missing Data for Single Loop Surveillance Systems. Transportation Research Record No. 1855, pp. 160–167.

Daganzo, C., 1994. The cell transmission model: a dynamic representation of highway traffic consistent with the hydrodynamic theory. Transportation Research Part B 28 (4), 269–287.

Daganzo, C., 1995. The cell transmission model, part II: network traffic. Transportation Research Part B 29 (2), 79–93.

Friesz, T., Mookherjee, R., Yao, T., 2008. Securitizing congestion: the congestion call option. Transportation Research Part B 42 (5), 407–437.

Frühwirth-Schnatter, S., 2006. Finite Mixture and Markov Switching Models. Springer, New York.

Geistefeldt, J., Brilon, W., 2009. A comparative assessment of stochastic capacity estimation methods. In: Lam, W., Wong, S., Lo, H. (Eds.), Transportation and Traffic Theory. Springer, pp. 583–602.

Gomes, G., Horowitz, R., 2006. Optimal freeway ramp metering using the asymmetric cell transmission model. Transportation Research Part C 14 (4), 244–262.

Gomes, G., Horowitz, R., Kurzhanskiy, A., Varaiya, R., Kwon, J., 2008. Behavior of the cell transmission model and effectiveness of ramp metering. Transportation Research Part C 16 (4), 485–513.

Kim, T., Zhang, H., 2008. A stochastic wave propagation model. Transportation Research Part B 42 (7–8), 619–634.

Li, J., Chen, Q., Wang, H., Ni, D., 2009. Analysis of LWR model with fundamental diagram subject to uncertainties. In: The 88th Transportation Research Board (TRB) Annual Meeting, Washington, DC (Pre-print CD-ROM).

Mohler, R., 1973. Bilinear Control Processes: With Applications to Engineering, Ecology, and Medicine. Academic Press, New York.

Muñoz, L., Sun, X., Horowitz, R., Alvarez, L., 2003. Traffic density estimation with the cell transmission model. In: Proceedings of the American Control Conference. Denver, Colorado, USA, pp. 3750–3755.

Mihaylova, L., Boel, R., Hegyi, A., 2007. Freeway traffic estimation within particle filtering framework. Automatica 43 (2), 290–300.

Nie, X., Zhang, H., 2005. A comparative study of some macroscopic link models used in dynamic traffic assignment. Networks and Spatial Economics 5 (1), 89–115.

Ngoduy, D., in press. Multiclass first order model using stochastic fundamental diagrams. Transportmetrica.

Peeta, S., Zhou, C., 2006. Stochastic quasi-gradient algorithm for the off-line stochastic dynamic traffic assignment problem. Transportation Research Part B 40 (3), 179–206.
Schönhof, M., Helbing, D., 2007. Empirical features of congested traffic states and their implications for traffic modeling. Transportation Science 41 (2), 135–166.
Sumalee, A., Pan, T., Zhong, R., Uno, N., submitted for publication. Dynamic stochastic journey time estimation and reliability analysis using stochastic cell transmission model: algorithm and case studies. Transportation Research Part C.
Sun, X., Muñoz, L., Horowitz, R., 2003. Highway traffic state estimation using improved mixture Kalman filters for effective ramp metering control. In: Proceedings of the 42nd IEEE Conference on Decision and Control. Hawaii, USA, pp. 6333–6338.
Szeto, W.Y., 2008. The Enhanced Lagged Cell Transmission Model for Dynamic Traffic Assignment. Transportation Research Record No. 2085, pp. 76–85.
Tuan, P., 1985. Bilinear Markovian representation and bilinear models. Stochastic Processes and Their Applications 20 (2), 295–306.
Wang, Y., Papageorgiou, M., Messmer, A., 2007. Real-time freeway traffic state estimation based on extended Kalman filter: a case study. Transportation Science 41 (2), 167–181.
Wang, H., Li, J., Chen, Q., Ni, D., 2009. Speed–density relationship: from deterministic to stochastic. In: The 88th Transportation Research Board (TRB) Annual Meeting, Washington, DC (Pre-print CD-ROM).
Zhang, H., Ritchie, S., Recker, W., 1996. Some general results on the optimal ramp control problem. Transportation Research Part C 4 (2), 51–69.
Zhong, R., Sumalee, A., Pan, T., Lam, W.H.K, submitted for publication. Stochastic cell transmission model for traffic network with demand and supply uncertainties. Transportmetrica.